Measurement of Heterogeneity in Low Consistency Pulp Refining by Comminution Modeling

by

Jens Olaf Heymer

Dipl.-Ing. (TU), The Dresden University of Technology, 2002

A THESIS SUBMITTED IN PARTIAL FULFILMENT OF

THE REQUIREMENTS FOR THE DEGREE OF

Doctor of Philosophy

in

The Faculty of Graduate Studies

(Chemical and Biological Engineering)

The University of British Columbia

(Vancouver)

June, 2009

Abstract

Pulp refining is a key operation in papermaking aimed at improving fibre quality for paper. In pulp refiners, pulp in suspension flows through an annulus between a rotor and stator having surfaces with bars which impose cyclic loading on the pulp during bar crossings. This process has long been known to be heterogeneous in its treatment of pulp. However, there is no method available to measure heterogeneity of treatment in operating refiners. The objective of this thesis was to develop such a method.

The approach was based on applying comminution theory and measurements of fibre length before and after refining. Specifically, measurements of fibre shortening were used to obtain two key parameters in the comminution differential equation: the selection function and the breakage function. A procedure was employed to account for breakage at any point along a fibre length instead of an arbitrary point as in previous studies. The selection function was expressed as the product of two factors: a probability of impact and a probability that intensity of an impacted fibre exceeded the rupture intensity. These probabilities were expressed in terms of refiner variables, with an increment of energy being a single bar crossing. Values for the selection and breakage functions were obtained by regression fitting to fibre length data. These length distribution data were obtained for a range of operating conditions in a pilot plant disc refiner, an industrial conical refiner, and a laboratory Escher Wyss refiner. Findings for predicted numbers of impacts and intensities were consistent with the findings of previous studies.

The probabilities derived from the selection and breakage functions gave distributions of numbers and intensities of impacts. The findings showed, for example, that homogeneity of treatment is more dependent on numbers of impacts than on uniformity of intensity

during impacts. A single number “homogeneity index” was proposed and defined as the product of the number of impacts on fibres having length-weighted average and the probability of intensity being within +/- 2kJ/kg of the mean divided by the specific energy. Using this definition, it was shown that homogeneity of refining treatment increased with flow rate through the refiner and decreased with increasing groove depth and consistency. It also showed the degree to which increased residence time of fibres in a refiner could compensate for a coarse bar pattern in attaining homogeneity of treatment.

Table of Contents

List of Tables

List of Figures

Nomenclature

a	Shape parameter for intensity distribution, $[kJ/kg]^{-1}$
A	Comminution matrix
A_F	Cross sectional area fibre, $[m^2]$
b	Scale parameter for intensity distribution, $[kJ/kg]^{-1}$
B	Breakage function matrix
B_{ij}	Breakage function, [-]
BL	Breaking length of paper, [km]
BEL	Breaking Edge Length, [km]
C	C-Factor, $[s^{-1}]$
C_F	Consistency pulp suspension, [%] or [-]
CEL	Cutting Edge Length, [km/s]
E	Energy input. [kWh/t]
dE	Incremental energy input, [kWh/t]
D	Groove Depth, [mm]
EM	Elastic Modulus (Young's modulus), [Pa]
$f(l_i)$	Probability of capture form of fibres of length l_i, [-]
F_{Ci}	Factor for fibres length i to be captured during one bar crossing event, [-]
F_{max}	Maximum force, [N]
G	Groove width, [mm]
H	Homogeneity index, [-]
I	Intensity of impacts, [kJ/kg]

I_A	Average intensity of impacts, [kJ/kg]
I_C	Critical rupture strength of fibres, [kJ/kg]
I_{CA}	Average critical rupture strength of fibres, [kJ/kg]
I_n	Identity matrix
K	Empirical constant depending on machine parameter, [-]
l_A	Average fibre length, [mm]
$\dot{m}$	Mass throughput of O.D. pulp, [t/h] or [kg/s]
m_G	Mass of fibres in the grooves per unit bar length, [kg/m]
m_T	Mass of fibres in the gap per unit bar length, [kg/m]
MEL	Modified Edge Load, [J/m]
$n(E)$	Column vector of fibre length classes at energy input level E
n_i	Numbers of fibre length class i, [-]
dn_i^*/n_i	Incremental shortening of fibres of length class i, [-]
$n^*_{Tracer,j}(E)$	Fraction of the number of tracer fibres in length class j, [-]
n_t	Initial state vector
N	Number of impacts on fibre, [-]
N_A	Average number of impacts, [-]
N_B	Number of bar crossings fibre experiences while traveling thr. refiner, [-]
N_C	Number of compression cycles, [-]
out_i	Estimated values according to Markovian transition matrix approach
P	Average probability of fibre capture for one bar crossing, [-]
$p_C(I_C)$	Rupture strength - probability distribution density function, [-]
$p_I(I)$	Intensity probability distribution density function, [-]

P_R	Probability of refining intensity exceeding the rupture strength of fibres, [-]
$p_{Gamma}(I)$	Gamma probability distribution density function, [-]
P_{net}	Net energy input, [kW] or [kJ/s]
Q	Volume throughput, [m^3/s]
R_1	Inner radius refiner [m]
R_2	Outer radius refiner, [mm]
RBA	Relative Bonded Area [-]
$R_D(E)$	Matrix of eigenvalues
$R(N_B)$	Fraction of fibres that have been captured and therefore treated, [-]
S	Selection function matrix
S_i	Selection function, [kWh/t]$^{-1}$ or [kJ/kg]$^{-1}$
SEL	Specific Edge Load, [Ws/m] or [J/m]
SRE	Specific Refining Energy, [kWh/t] or [kJ/kg]
SSL	Specific Surface Load, [Ws/m^2] or [J/m^2]
t	Energy state, [kWh/t], or [kJ/kg]
$t(j, i)$	Probability transition matrix
$T.E.A.$	Tensile energy absorption [J/m^2]
U_T	Matrix of the eigenvectors
v_{ij}	Elements of $V(E)$
$\dot{V}$	Volume flow through the refiner, [m^3/s]
$V(E)$	Transition matrix
w	Fibre coarseness, [mg/m]
W_R	Bar Width of the Rotor, [mm]

W_S	Bar Width of the Stator, [mm]
x	Number of Bins of fibre length measurement, [-]
α	Shape parameter for gamma distribution function, [-]
α_B	Bar angle, [°]
β	Scale parameter for gamma distribution function, [-]
δE	Small energy input, [kJ/kg]
ε	Elastic strain at failure, [-]
θ	Sector angle refiner plate, [-]
k	Shape parameter for Weibull probability distribution function, [-]
λ	Scale parameter for Weibull probability distribution function, [-]
μ	Learning rate parameter
ρ	Density fibre, [kg/m^3]
σ	Stress (tensile strength), [N/m^2] or [Pa] or [10^1 dyne/cm^2]
υ	Poisson ratio, [-]
ϕ	Bar angle, [°]
ω	Rotational speed, [rev/min] or [rev/s]

Acknowledgments

I would like to thank my supervisors James Olson and Richard Kerekes for providing strong leadership, inspiration, and support over the course of my Ph.D., and for showing me what it takes to bring an academic quest through to completion. I would also like to thank my committee members Mark Martinez and Chad Bennington for their help and advice in this project. I wish also to acknowledge my co-researchers and staff of the pulp and paper centre at UBC for their work ethic and encouragement, namely Sean Delfel, Paul Krochak, Tim Paterson, and Ken Wong.

It was absolutely necessary to have a supportive network of friends and family to help me on my journey through this project. My deepest thanks to those in my life who always supported and encouraged me over the past years.

Grateful acknowledgement is made for financial and technical support from NSERC, CANFOR, STORA ENSO and FPInnovations, Paprican Division.

1 Introduction

Pulp refining is one of the most important unit operations in papermaking. Its purpose is to modify fibre morphology in order to improve paper properties by a technology which has developed from batch beaters in the early 19th century to flow-through disc, conical, and cylindrical refiners in use today. In pulp refiners fibres are trapped in the gaps between bars during bar crossings during pulp flow through an annulus between a rotor and stator which have bars on their surfaces, and subjected to cyclic compression and shear forces which modify fibre properties.

The result of refining is changes in physical and optical properties of paper have been studied in detail by various authors over the past decades (Higgins and de Yong/1962[1], Page/1985[2], Seth/1996[3] and Hiltunen et al./2002[4]) to name only a few). It has been generally found that, within the commercial range, refining increases tensile strength (about threefold), burst strength, folding endurance, and sheet density, whereas it reduces tear strength of paper and sometimes fibre length.

Although there is extensive literature on changes in fiber morphology produced by refining, there is relatively little on how the refining action takes place, that is, on the refining process itself (Atack/1980[5], Page/1989[6]). Consequently, quantitative characterization of refining action is limited. The most widely used quantitative measure of refining action is net energy expended per unit mass, i.e. specific refining energy (*SRE*). In addition, it is common to use a "refining intensity" which reflects the energy expended per loading cycle at each bar crossing event. However, although useful, energy-based characterizations have limitations because most changes within fibres occur as a

result of forces, not energy. The use of force in characterizing refining action has only recently been undertaken (Kerekes and Senger/2006[46]).

It has long been known that refining is very non-uniform in its treatment of pulp (Danforth/1986[7]). However, the causes and consequences of this heterogeneity have been little studied. Furthermore, heterogeneity of treatment has not been taken into account in any of the refining theories or characterizations, due in good part to a lack of means to measure heterogeneity. Thus, it is reasonable to expect that a better understanding of the nature of heterogeneity in refining will lead to a better understanding of the process and perhaps offer a basis for improved technology.

The objective of this dissertation is to develop a method to measure heterogeneity of treatment in operating refiners.

2 Review of Literature

Several excellent reviews of pulp refining have been produced over the years. Generally they have emphasized changes in fibre morphology caused by refining, for example: Higgins and de Yong/1962[1], Page et al./1962[8], Atack/1977[9], Page/1985[2], Seth/1996[3] and Hiltunen et al./2002[4]). The fundamentals of the refining process have also received study, as shown in the reviews of Ebeling/1980[10], Page/1989[6], Hietanen/1990[11] and Hietanen and Ebeling/1990[12]). The following review of the literature will focus on highlights from past studies relevant to heterogeneity of treatment.

2.1 Effect on Pulp

The main effects of refining on pulp are: internal fibrillation, external fibrillation, fibre shortening and fines generation. More recently, fibre straightening has been recognized as another primary effect by Page/1985[2], Mohlin and Miller/1995[13] and Seth/2006[14]. These outcomes of refining are described below in more detail.

2.1.1 Internal Fibrillation

Measurements by Mohlin/1975[15], Kerekes/1985[16] and Paavilainen/1993[17] have shown that refining chemical pulp increases fibre flexibility. This occurs from delamination in the cell wall, which lowers its effective elasticity. Water is drawn into the fibre walls by capillary forces, causing swelling which is often used as an indicator of degree of refining. The weakened cell wall is more flexible and collapsible, thereby giving a larger relative bonded area in paper. This in turn increases bonding and thereby paper strength.

2.1.2 External Fibrillation

Another effect in commercial refining is the delamination of fibre surfaces, called external fibrillation. This can be defined as a peeling off of fibrils from the fiber surface, while leaving them attached to the fiber surface (Page et al./1967[18], Page/1989[6]). Clark/1969[19] emphasized that the fiber surface can be fibrillated even in the early beating stage, and that the external fibrils serve as bonding agents for inter-fiber bonding. The amount of such fibrillation (parts of fibre wall still attached to fibre) can be quantified by measuring the increase in the specific surface of the long fibre fraction (Page/1989[6]). Although external fibrillation was studied from the earliest years of refining because it was easily observable under microscope, and was thought to be the dominant result of refining, several modern authors, i.e. Page/1985[2] and Hartman/1985[20] concluded that external fibrillation has only limited effect on the tensile strength or elastic modulus.

2.1.3 Fibre Shortening

Refining causes fibre shortening which is generally undesirable in refining. In some rare applications it is a desired effect to improve formation by decreasing the crowding number (Kerekes/1995[21]). In early work, Page/1989[6] showed that the mode of fibre shortening was tensile failure rather than “cutting” by scissor-like shearing.

2.1.4 Fines Generation

Fines, meaning loose fibrous material of size less than 0.3 mm, are produced in refining as a result of fibre shortening or removal of fibrils from fibre walls. According to

Page/1989[6], generated fines consist mostly of fragments of P1 and S1 layers of the fibre wall due to the abrasion of fibres against each other or against refiner bars.

2.1.5 Fibre Straightening

Fibre straightening is considered an important refining effect (Page/1985[2], Mohlin/1991[22], Seth/2001[23]). If fibres remain curly or kinked in a paper network, they must be stretched before they can carry load, meaning that fewer fibres carry load during the initial stretching of paper, and therefore paper is weak. Fibre straightening permits fibre segments between bonded sites in paper to be "active" in carrying load. The mechanism by which refiners straighten fibres is likely due in part to tensile strain in refiner gaps and by causing fibre diameter swelling. In the latter case, upon drying, shrinkage of swollen fibres stretches fibres segments between bonded sites and thereby straightens them.

2.1.6 Heterogeneity

It has long been known that refining is a heterogeneous process and that the resulting heterogeneity affects paper properties. One of the earliest workers to show this was Danforth/1986[7] by mixing of fibres subjected to differing levels of refining. Larger heterogeneity gave poorer properties, e.g. lower tensile strength. Others have shown heterogeneity by observations of morphology changes (Page/1989[6]). The literature on heterogeneity will be reviewed extensively later in section 2.6.

2.2 Mechanics of Refining

Current knowledge of the mechanics of refining is far less than is knowledge of the refining result. The design of refiners is largely empirical. In addition to action on pulp,

design is based on factors such as sufficient groove size to permit flow of the fibre suspension through the machine, bar wear, and material cost. Scientific studies of the process of refining have been carried out by various researchers. Some highlights of this past work are described below.

2.2.1 Fibrage Theory

Smith/1922[24] proposed that a refiner bar moving through stock collects a "beard" or fibrage of fibers on the leading edge. This capture of fibre transports fibres into the gap between rotor and stator bars. A study of the compressive and shearing forces exerted on the bars during refining by Goncharov/1971[33] gave some support to the fibrage mechanism.

2.2.2 Refining as Lubrication Process (Hydrodynamics)

Rance/1951[25] and Steenberg/1951[26] analyzed refining as a lubrication process. Their experiments offered indirect evidence of the occurrence of (a) fluid (hydrodynamic) lubrication, (b) boundary lubrication, and (c) lubrication breakdown, which produced excessive metal wear in the refiner. Steenberg/1951[26] carried out his experiments with a Valley beater varying the consistency, load and peripheral speed. He concluded that Valley beating is carried out under hydrodynamic (fluid) lubrication conditions and that the work absorption capacity, i.e., coefficient of friction, decreases with beating as does the apparent viscosity of the pulp. More recently Frazier/1988[27] applied the lubrication theory to refiner mechanical pulping and derived an expression for the shear force applied to pulp. Similarly Roux/1997[28] performed a lubrication analysis in order to characterize hydrodynamic forces in refining. Based on experiments Lundin et al./1999[29] propose

that the power consumption in refining is governed by a lubrication film between the rotor and the stator. Although characterization of the refining process as a hydrodynamic phenomenon has yielded some useful correlations, treating the fibre suspension as a fluid has some serious limitations. Refiner gaps are 5-10 fibre diameters deep and therefore the water-fibre suspension in a gap is not a continuum. Consequently the suspension in the gap does not meet a primary property of a fluid.

2.2.3 Transport Phenomena in Refiners

Flow behavior in refiners has been examined by several workers. Complex flow patterns have been observed and residence time distributions have been measured using high speed photography (Halme and Syrjanen/1964[30], Herbert and Marsh/1968[31], Banks/1967[32], Gonchorov/1971[33], Fox et al./1979[34] and Ebeling/1980[10]). Halme and Syrjanen/1964[30], Herbert and Marsh/1968[31] observed that pulp flows primarily in the radial direction outward in the grooves of the rotor and inward in the grooves of the stator. Other recirculation flows, called secondary and tertiary flows, are also present in disc refiners. Fox et al.[34] proposed that the secondary flows arise from the motion of the land area of the bars passing over the grooves and that tertiary flows result from the difference in static pressure between opposing grooves of the rotor and stator (see Figure 1). Using a material and energy balance, Leider and Rihs/1977[35] and Leider and Nissan/1977[36] related the pressure drop across the refiner to its volumetric flow rate. This accounts for the action of the centrifugal and frictional forces and is expressed in terms of operating conditions, fluid properties and plate properties.

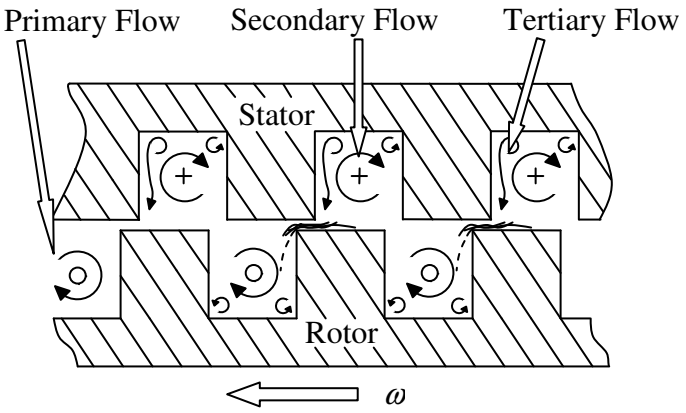

Figure 1: Pulp flow pattern within the refiner plate by Fox/1979[34,37]

Arjas et al./1969[38] studied the effect of flow rate and angular velocity on the shape of the residence time distribution curve. They concluded that the flow rate has an effect on the mean residence time, but the effect of the angular speed is not very large.

2.2.4 "Treatment of Flocs" Hypothesis

Page et al./1962[8] showed that flocs rather than individual fibres are treated in refining , although it is possible that fibers may be oriented in a floc network to receive fiber treatment. From high-speed photography of a conical refiner, they concluded that a refiner is inefficient since only a small proportion of fibers are subject to treatment. Page et al./1962[8], Hietanen and Ebeling/1990[12] found that flocculation plays an important role in low-consistency refining. Similarly, studying power and gap size relationships, Batchelor & Ludin/2006[39] estimated the fraction of bar length covered with fibres.

Banks/1967[32] proposed a detailed picture of refining action based on floc treatment in contrast to the fibrage theory which assumes a uniform coverage of the bar edges by

individual fibres. He summarized the mechanics of refining based on observations using high-speed photography:

1. Flocs consolidate when they are trapped between approaching tackle elements.

2. Mechanical pressure induced by the tackle elements becomes high enough and causes plastic deformation in the fibers composing the floc. Consolidation continues.

3. The floc compressed between the bars is sheared; flocs (and fibers) are ruptured.

4. Release of mechanical pressure allows absorption of water to take place into the ruptured fibrils and fibers.

5. Turbulent agitation may disperse the floc or its remnants into the general mass flow.

2.2.5 Refining as a Fatigue Process

Fibres may be exposed to many bar crossing events during their passage through a refiner. Thus, fibres are likely to experience multiple loading cycles. Page et al./1962[8] and Atack/1977[9] suggested that this repeated straining causes fatigue weakening of the fibres, and this in turn produces internal fibrillation. On the other hand, fibre shortening (cutting) is likely to be caused by one severe loading cycle. Page/1989[6] suggested rupture takes place by tensile failure rather then a scissor-like cutting action. Kerekes and Olson/2003[40] proposed that fibre rupture in refiners is caused by a single event rather than fatigue process.

Another approach to account for the cyclical nature of the process was proposed by Steenberg/1979[41]. He considered the refining process to be an irreversible *kappa*

process, in which there is a critical path for the formation of a stress concentration chain, which causes a structural breakdown. For another structural breakdown to occur the particles, i.e. fibers, need to be rearranged. Thus cyclicality is needed to overcome heterogeneity. Most recently, Goosen et al./2007[42] examined the role of fibre redistribution in pulp refining by compression. They concluded that the role of cyclic loading is to expose new fibres to loading cycles rather than to produce fatigue weakening. In essence, cyclicality in the process is to overcome heterogeneity rather then to produce fatigue weakening.

2.2.6 Forces on Fibres during Bar Crossing Events

A number of studies have examined the manner in which forces are imposed on fibres within refiner gaps. Page/ 1989[6] suggested that refining should be quantified by the stresses and strains applied to fibres. These stresses and strains are caused by bar forces which have been the subjects of several studies.

Goncharov/1971[43] was the first to measure pressures on refiner bars during bar crossing events. Later Martinez et al./1997[44] and Batchelor et al./1997[45] analyzed the compressive and shear forces action on single flocs and measured normal and shear forces in a "single bar" refiner apparatus. Kerekes and Senger/[46] developed equations for bar forces and fibre forces from the specific edge load (*SEL*). Page/1989[6], Martinez et al./1997[44] and Koskenhely et al./2007[47] addressed issues concerning the bar edge force.

2.3 Quantitative Characterization of the Refining Mechanism

As described earlier, specific refining energy is the most common quantitative characterization of refining action. This energy is factored into the number of impacts imposed on pulp and the intensity of each impact, i.e. loading cycle. Most intensities are based on energy per loading cycle, though in recent work Kerekes and Senger/2006[46] have proposed a force-based intensity. These concepts are described in detail below.

2.3.1 Specific Energy

Specific refining energy (*SRE*) is the useful energy imparted to the pulp suspension, i.e. the total energy less the no-load energy. It is obtained by dividing the net power input into the refiner by the fibre mass throughput.

$$SRE = \frac{P_{net}}{\dot{m}} = \frac{P_{net}}{C_F \cdot \dot{V} \cdot \rho} \tag{1}$$

The typical range for *SRE* in chemical pulp refining is between 80 to 250 kWh/t, depending on the furnish and the desired papermaking property.

2.3.2 Refining Intensity

The major means of characterizing refining intensity today is by a “machine intensity”, meaning an intensity which reflects energy expended per bar crossing without direct reference to how this energy is expended pulp. The most common such method is the Specific Edge Load (*SEL*). This was introduced by Wultsch and Flucher/1958[48] and developed further by Brecht and Siewert/1966[49] who demonstrated the dominant impact of the bar edge. The *SEL* is determined by the net power divided by the bar edge length (*BEL*) multiplied by the rotational speed ω. The *BEL* is determined by multiplying the

number of bars on stator by the number of bars on rotor by the refining zone length. The result is expressed in Ws/m or J/m. The expression for *SEL* is:

$$SEL = \frac{P_{net}}{BEL \cdot \omega} = \frac{P_{net}}{CEL} \tag{2}$$

$$BEL = \int_{R_1}^{R_2} \frac{n_r \cdot n_s \cdot r}{\cos\theta} \cong \sum_{1}^{N} \frac{n_r \cdot n_s \Delta r}{\cos\theta} \tag{3}$$

An extension of the *SEL*, the specific surface load (*SSL*), was suggested by Lumiainen/1990[50] to account for bar width rather than just bar edges. This was accomplished by including bar width *W* with the *SEL*, thereby giving the area of the bars and units Ws/m^2 or J/m^2.

$$SSL = \frac{P_{net}}{CEL \cdot \omega \cdot \left(\frac{W_R + W_S}{2 \cdot \cos(\alpha_B / 2)} \right)} \tag{4}$$

Using this approach Lumiainen distinguished between refiner plates having identical cutting edge length (*CEL*) but differing bar widths.

Meltzer and Rautenbach/1994[51] used the "crossing speed" – which is a measure of fibre treatment frequency by calculating the crossing speed per dry fibre mass flow – to further modify the *SEL*-concept. This gave the modified edge load (*MEL*) which accounts for bar width, *W*, groove width, *G*, and the average intersecting angle of rotor and stator bars. For identical rotor and stator geometry the following expression was derived:

$$MEL = SEL \cdot \frac{1}{2 \cdot \tan\alpha_B} \cdot \frac{W + G}{W} \tag{5}$$

The factor *W+G / W* considers the refining work of the bar surfaces and the probability of fibre treatment received.

2.3.3 Fibre Intensity

The above characterizations based on energy per bar crossing are "machine intensities" that make no direct link to the pulp in the refiner. To make this link, characterizations have been developed that factor *SRE* into two quantitative parameters: the number of impacts, *N*, and the intensity of each impact, *I* on pulp. In this case, *I* is a "fibre intensity". The product of these in the SRE are shown in equation (6).

$$SRE = N \cdot I \tag{6}$$

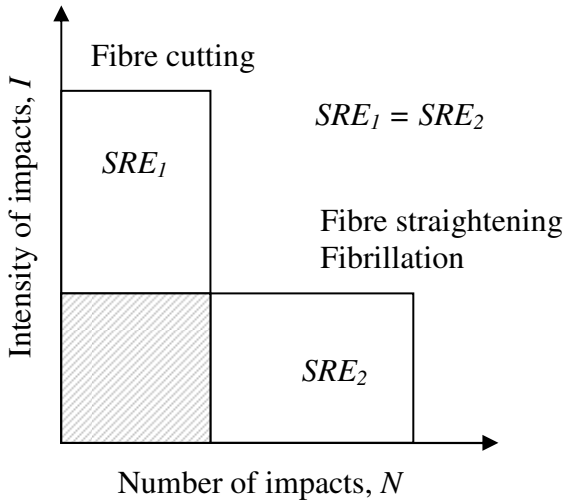

Figure 2: Same amount of energy imparted into fibres in two ways

As shown in Figure 2 differing combinations of *N* and *I* give differing refining results. Because only 2 of the variables in equation (6) are independent, it is common to use *SRE* and *I*. Lewis and Danforth/1962[52] and later Danforth/1969[53] defined expressions for *N* and *I*, but these were empirical in nature and did not rigorously represent *N* as a dimensionless variable and *I* as energy per bar per impact.

Van Stiphout/1964[54] calculated the probability of a fibre being caught in the refiner gap. Based on this he was able to estimate the forces acting on fibres and the mass of fibres being treated per length of bar. According to his analysis the mass of fibres per bar length was proportional to the mean residence time. He further postulated that the damaging affect of refining was proportional to the surface sheared and that the net power was active on an amount of fibres enclosed in the gap between the refiner bars. However, two empirical parameters of unknown magnitude limited the application and scientific meaning of this work.

Leider and Nissan/1977[36] were the first to derive equations for *N* and *I* in rigorous terms. They represented the probability of a fibre being stapled on a bar by fibre length and diameter to give an estimate of "number of impacts per single fibre per refiner pass". Another approach to define values for *N* and *I* to overcome some of the shortcomings of Leider and Nissan was made by Kerekes/1990[55] in the form of the C-factor.

$$SRE = \frac{P_{net}}{\dot{m}} = N \cdot I = \frac{C}{\dot{m}} \cdot \frac{P_{net}}{C} \tag{7}$$

In this approach, *C* is defined as the capacity of a refiner to inflict impacts (loading cycles) on fibres. Kerekes/1990[55] derived equations for the *C*-factor as a function of plate geometry (bar width, depth, length, angle, and edge geometry), speed, consistency, fiber length, and coarseness. The *C*-factor for a disc refiner for a simplified case (small gap size, similar bar pattern on rotor and stator), is given by:

$$C = \frac{8\pi^2 GD\rho C_F l_A \cdot n^3 \omega (1 + 2\tan\phi)\left(R_2^3 - R_1^3\right)}{3w\left(l_A + D\right)} \tag{8}$$

A crucial assumption of the analysis is estimating the probability of fiber contact with the leading edge of the bar, which he expresses as *l / (l + D+ T)*. Kerekes showed that this

assumption led to logical outcomes at the limits of bar size relative to fibre length. The *C*-Factor analysis is perhaps the most rigorous and comprehensive theory developed to date. It has been applied to a variety of refiner geometries including the disk, conical, and PFI mill. It takes into account factors relating to bar and groove geometry as well as fibre length, which provide a more accurate description of refining intensity. However, the *C*-factor predicts only average values rather than distributions of intensity.

2.4 Heterogeneity

It has long been accepted that refining is a heterogeneous process (Page/1989[6]). The sources of heterogeneity are numerous, ranging from: the mechanism of transferring mechanical forces into fibers (Steenberg/1963[56]) to the irregular flow pattern through the refiner (Halme/1962[57]).

There are also scales of heterogeneity ranging from large to small. Ryti and Arjas/1969[58] studied the large distributions of residence time in refiners, originating from large scale secondary flows. They postulated that greater uniformity in refining treatment gives a better refining result. They concluded that the refining action is related to the residence time inside the refiner and to the probability of treatment during this time. Fox et al./1979[34] studied flow in a small disc refiner by visual observation. They found that after being "released" from a gap, fibres either become part of the stator flow towards the refiner axis and stapled again on a bar, or become part of the outward rotor flow leaving the refiner. In addition fibres may flow back to the stator from the outside annulus of the refiner. This all resulted in a poor pulp circulation and therefore limited the amount of fibres receiving treatment in refiner gaps.

Additional sources of heterogeneity arise from a finite probability of capture from the groove (Olson et al./2003[59]), fractional bar coverage (Batchelor and Ludin/2006[60]), non-uniform force distribution within flocs (Batchelor and Ouellet/1997[61]), non-uniform *SEL* along the radius of the refiner (Roux and Joris/2005[62]), non-homogeneous force distribution on fibre networks while being under load (Endres et al./2005[63]), and out-of-tram of rotors (Prairie et al./ 2007[64]). An added complexity is the wide variability of fibre properties in any pulp. It is well known that species, pulp type, bleaching process, and the relative amounts of thick and thin walled fibers can affect refining. Page/1983[65] has suggested that differences in the beatability and refining action of kraft and sulfite pulps are due to differences in their viscoelastic behavior. Yet another factor is fibre flocculation. Hietanen and Ebeling/1990[12], Hietanen/1991[66] and Lumiainen/1995[67] have all suggested that flocculation is a major source of refining heterogeneity.

Various studies have been conducted to measure heterogeneity of treatment in refining. Simons/1950[68]) used a staining technique to identify damaged fibres. Nisser and Brecht/ 1963[69] evaluated refining heterogeneity by calculating the swollen length of fibres before and after refining. Another approach has been to examine physical changes in fibres. Mohlin and Librandt/1980[70] using SEM technique found that one of the major differences between laboratory refining and production refining is the homogeneity of treatment. Dahrni and Kerekes/1997[71] measured deformations in plastic tracer fibres. They found that 30% of the fibre passed through a lab disc refiner with no visible sign of impact whereas other fibres were severely deformed. Dekker/2005[72] measured the changes in *RBA* of fibres, by quantifying the optical contact between fibres and a glass slide. He found that only 7-20% of fibres were treated.

Another approach for measuring heterogeneity is based on comparing properties of papers made from mixtures of unrefined and well-refined pulp (Dillen/1980[73]). As a measure of the heterogeneity he used the coefficient of variation of the amount of refining. Lastly, Hietanen/1991[66] found that the homogenizing effect of deflocculation has a positive impact on paper strength properties.

In summary, the sources of heterogeneity in refining are many and there are some methods to measure it, but no existing methods are suitable for measurement of heterogeneity of treatment in operating refiners.

2.5 Review of Refining Action as a Comminution Process

Comminution is defined as the reduction of particle size by mechanical processing. Models for the comminution process models were developed for crushing and grinding in the powder industry 60 years ago to predict particle size distribution changes during processing. The basics were developed by Epstein/1948[74], Reid/1965[75] and Austin/1971[76]. They modeled batch grinding by the introduction of two statistical functions, a Breakage function, B_{ij}, and a Selection function, S_i. Basically S_i represents the probability of a particle of size i per unit time or energy and has the units of time^{-1} or energy^{-1}. The breakage function B_{ij} represents the probability of particles larger than i being reduced to size i. As the particle size can only be reduced during grinding, the values of B_{ij} are dimensionless and range between 0 and 1.

The incremental change in the number of fibres of length i, dn_i, per incremental applied energy dE is given by the comminution equation shown below:

$$\frac{dn_i}{dE} = -S_i n_i + \sum_{j>i} B_{ij} S_j n_j \tag{9}$$

Applied to refining, n_i represents the number of fibres of length i available for cutting. S_i is the selection function for fibres of length i per unit energy. The product of S_i and n_i; represents the decrease in number of fibres of length i. The term $\Sigma B_{ij} S_j n_j$ represents the increase in the number of fibres of length i per unit energy from the cutting of fibres of lengths larger than i.

For refiners, we may consider incremental energy to be the discrete event of a single bar crossing assuming this to inflict a single loading cycle on fibres and fibres to be ruptured by a single excessive loading cycle.

Steenberg/1963[56] suggested that several sub-processes have a major influence on the refining result during certain phases of refining. Thus a single parameter cannot be used to describe either the process or the state of the product (i.e. refined pulp). He suggested that at least two of the sub processes, namely the "selection process" and the "treatment process", deserve more attention.

Other workers applied the model directly to describe fibre length distribution changes caused by refining, for example Kane/1957[77] and Meyer et al./1966[78]. Roux and Mayde/1997[79] applied the comminution theory to analyze the change of the mean fibre length during refining. They predicted the potential for fibre cutting under given conditions to be a function of the energy consumed by the solid phase and the average impact intensity, i.e. the ratio between the net machine power and the "cutting" length of

bars per unit time. However, their equations had inconsistent units, making their results difficult to interpret rigorously.

Corte and Agg/1980[80] used a comminution model to compare the shortening rate of fibres in a disc refiner and a laboratory beater. They found that the disc refiners cut long fibre more rapidly than short fibres, while a laboratory beater cut long and short fibres at the same rate. Olson et al./2003[59], applying a technique developed by Koka and Trass/1988[81], found that the probability of fibres being selected for cutting during refining is proportional to the applied energy and fibre length, and was independent of consistency. Regression fitting that minimizes the difference between measured and predicted fibre length distributions was used to determine the selection function, S_i, for various pulp and refiner combinations.

Several other investigators applied the comminution theory to the production of mechanical pulp in chip refiners. Corson/1972[82] modeled the refining of wood chips into individual fibres using a comminution approach. This approach was used more recently in an expanded form by Strand and Mokvist/1989[83] to model the operation of a chip refiner employed in mechanical pulping of wood chips.

3 Objective of Thesis

The above review shows that there is a need for a rigorous, practical method to measure heterogeneity in operating refiners. The objective of this thesis is to develop such a method. The approach is based on interpreting measurements of fibre shortening by a model of the physical process of refining described by comminution theory.

4 Analysis

Comminution modeling is a potentially useful basis for measuring heterogeneity for several reasons. Fibre shortening obviously reflects the probabilistic nature of refining because some fibres are shortened while others are not. The result, decreased fibre length, is a measurable change for which instruments for rapid measurement are now available. Lastly, the best tracer particles to reflect what happens to fibres are fibres themselves.

Fibre shortening is generally not an objective of refining. Indeed, it is to be avoided in most cases. In this study, fibre shortening will be used merely as an event to characterize the mechanics of the process rather that as a desired outcome. We employ comminution theory as the scientific basis of our approach. To do so, we address several individual problems:

- interpretation of comminution equation
- link to refiner mechanics
- probability of fibre capture in a gap
- probability of fibre shortening in a gap
- link between breakage function and selection function

4.1 Interpretation of Comminution Equation

As discussed earlier, the comminution equation reflects the net change in the number of fibres of size *i*, as the result of the decrease size *i* caused by shortening and the increase caused by fibre shortening from larger sizes.

$$\frac{dn_i}{dE} = -S_i n_i + \sum_{j>i} B_{ij} S_j n_j \tag{10}$$

However, our specific interest in this work is only the shortening component of comminution. Therefore, we focus on the first two terms of the comminution equation. We define the incremental shortening, as dn_i^*, to differentiate it from the net shortening dn_i in equation (10). Rearranging terms, we obtain:

$$\frac{dn_i^*}{n_i} = -S_i \cdot dE \tag{11}$$

In essence, this equation relates the incremental fraction of fibres of length *i*, (dn_i^* / n_i) that are shortened to the product of the selection function, S_i and the incremental energy supplied, dE.

We now consider $S_i \cdot dE$ in terms of refiner variables, specifically to fibre rupture during a single bar crossing. The probability of fibre rupture is the product of two other probabilities: a factor of fibre capture from the groove, F_{Ci} and the probability that once captured, the fibre is ruptured, P_R. We consider P_R, the probability that the intensity a fibre sees is greater than its rupture strength (intensity), to be independent of fibre length. Thus we may express $S_i \cdot dE$ as

$$S_i \cdot dE = F_{Ci} \cdot P_R \tag{12}$$

We now link dE, F_{Ci} and P_R to refiner mechanics and thereby refiner variables.

4.2 Link to Refiner Mechanics

We first link energy per mass supplied to a refiner *E*, to the product of number of impacts imposed on fibres, *N*, and the intensity per input *I*, expressed as energy per mass.

$$E = N \cdot I \tag{13}$$

We may express this equation in incremental form as

$$dE = N \cdot dI + I \cdot dN \tag{14}$$

Assuming that for a given refiner, the average intensity at bar crossings is constant and represented by I_A, and since $dI = 0$, we obtain

$$dE = I_A \cdot dN \tag{15}$$

4.2.1 Intensity

We now interpret *N* and I_A in terms of measurable refiner variables at a single bar crossing.

Refining intensity is commonly defined by the Specific Edge Load (*SEL*). Kerekes and Senger/2006[46] have shown that *SEL* represents the energy expended per bar crossing per unit bar length. Thus, the average energy expended on fibre mass within the gap of a bar crossing, I_A, is given by *SEL* divided by the mass of fibres in the gap per unit bar length, m_T, i.e.

$$I_A = \frac{SEL}{m_T} \tag{16}$$

4.2.2 Number of Impacts

The number of impacts on pulp, *N*, is a function of the product of two factors: the probability of an impact at a single bar crossing and the number of bar crossings N_B that a

fibre would experience if it passed along a stator bar during its residence time in the refiner. We can define a mass-average probability of impact at a bar crossing by the ratio of the mass of pulp captured, m_T to the total mass associated with a bar crossing (pulp in gap and pulp in adjacent groove, m_G), giving $m_T / (m_T + m_G)$. Thus

$$dN = m_T / (m_T + m_G) \cdot dN_B \tag{17}$$

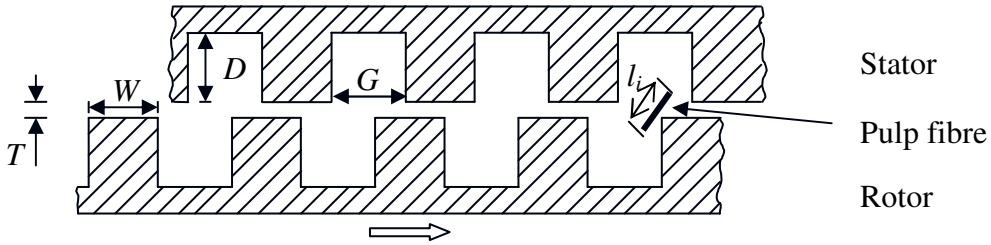

Figure 3: A representative refiner bar pattern showing bar and fibre dimensions.

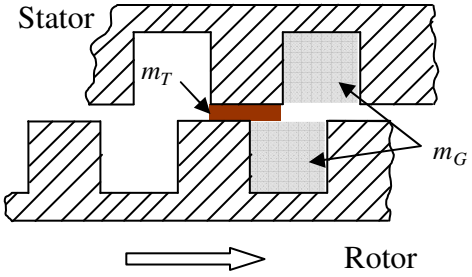

Figure 4: Plate pattern showing mass location

We assume that the consistency in refiner grooves equals the pulp suspension consistency, C_F. Thus

$$m_G = 2 \cdot \mathrm{D} \cdot \mathrm{G} \times \mathrm{C_F} \times \rho \tag{18}$$

We may note here that the above equations give the following equation when combined:

$$E = N \cdot I_A = \frac{m_T}{m_T + m_G} \cdot N_B \cdot \frac{SEL}{m_T} = \frac{N_B \cdot SEL}{m_T + m_G} \tag{19}$$

These expressions represent averages. We now consider distributions.

4.3 Fibre Capture Factor

The above mass-average probability of capture assumes a dependence only on mass ratio. However, other factors also affect fibre capture. For example, the mass in a groove may not reflect eligible fibres because there may be dead zones of inactive fibres stuck in the groove. This would be a source of heterogeneity. In addition, it has long been known (Smith/1922[24]) that longer fibres tend to be more easily captured then short fibres, individually or as flocs. To reflect these factors, we express the factor of capture as a probability based on fibre length, $f(l_i)$, and a constant K that reflects other unknown factors influential in capture, such as consistency, rotational speed, throughput and plate geometry. Clearly K falls in the range $0 \le K \le 1$ .Thus

$$F_{Ci} = K \cdot f(l_i) \tag{20}$$

4.4 Probability Distribution of Intensity

Once in a gap, fibres rupture when they experience a force exceeding their rupture strength. We consider forces to be represented by intensities expressed as energy per unit mass. Thus, the probability of fibre rupture depends on the intensity applied to a fibre, I, and the rupture intensity, I_C. We further assume that, once captured, rupture is independent of fibre length.

We assume the distribution of intensity, I, on a pad of pulp to be similar to the spatial pressure distribution measured by Endres et al./2005[63]. In this work, Endres measured local pressure distributions on pads of wet pulp in increments of a few mm, i.e. 8 x 8 mm. In a refiner gap, compression forces are large, about 10 times the shear forces (Prairie et al./2007[64]), and therefore are likely to vary in a similar manner to the measurements of Endres along bar length in gaps, even in the presence of shear forces. In the absence of

other information of local forces in refiner gaps, we deemed this to be a reasonable assumption. As shown in Appendix B, the intensity density distribution can be described by Weibull function, and more approximately, by a simple form of the Weibull equation, the gamma density distribution, as shown below

$$p_I(I) = aIe^{-bI} \tag{21}$$

The constants a and b can be determined from two equations, one normalizing the distribution to 1 the other integrating the distribution multiplied by I to give the average intensity I_A, as shown in Appendix B. This gives

$$p_I(I) = \frac{4 \cdot 1[kJ/kg]}{(I_A)^2} \cdot Ie^{-\frac{2}{I_A} \cdot I} \quad \text{where } I_A = SEL/m_T \tag{22}$$

The strength of fibres, I_C, also has a distribution. We represent this distribution as $p_C(I_C)$. As shown in Appendix C, this too can be represented by a Weibull density distribution.

We now relate P_R in equation (12) to above probabilities. Clearly, rupture occurs when the applied intensity I equals or exceeds fibre rupture intensity I_C, summed over all fibre rupture intensities. This is given by:

$$P_R = \int_0^\infty \int_{I_C}^\infty p_I(I) \cdot p_C(I_C) \cdot dI \cdot dI_C \tag{23}$$

Solving the double integral of equation (23) does not give a simple general analytical solution owing to the complexity of the probability distribution functions in use: $p_I(I)$ as a Gamma density distribution function and $p_C(I_C)$ as a Weibull density distribution function. It has the form:

$$P_R = \int_0^\infty p_C(I_C) \cdot \frac{(2 \cdot I_C + I_A) \cdot e^{-\frac{2 \cdot I_C}{I_A}}}{I_A} \cdot dI_C \tag{24}$$

$$P_R = \int_0^{\infty} \frac{k}{\lambda^k} \cdot {I_C}^{k-1} \cdot e^{-\left(\frac{I_C}{\lambda}\right)^k} \cdot \frac{(2 \cdot I_C + I_A) \cdot e^{-\frac{2 \cdot I_C}{I_A}}}{I_A} \cdot dI_C \tag{25}$$

The solution of equation (25) is a hyper geometric function, for which examples for two different rupture strengths are shown Figure 5.

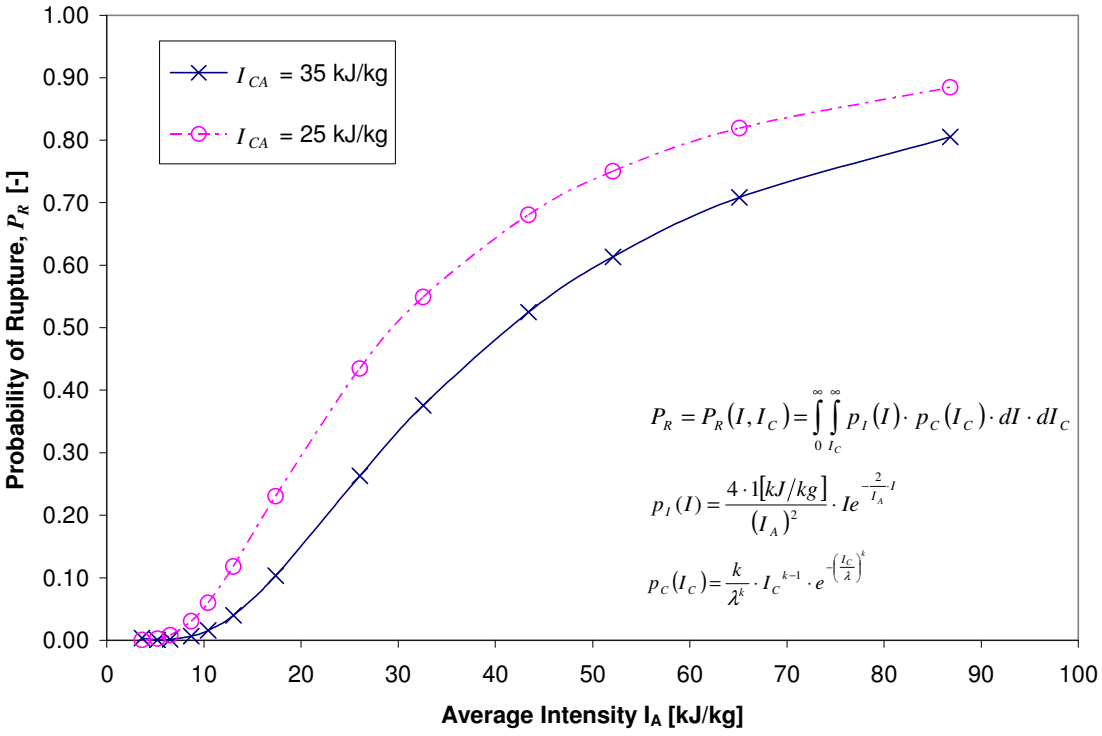

Figure 5: Probability that upon being captured, the average intensity I_A exceeds the rupture strength I_C of two different pulp fibres

4.5 Selection Function Expressed in Terms of Refiner Variables

We now link the above probabilities to the selection function, S_i. We do so by substituting F_{Ci} from equation (20) and P_R from equation (23) into equation (12). We obtain dE by substituting in equation (15) for I_A from equation (16) and for dN from equation (17). Assuming $m_T \ll m_G$. (Batchelor and Lundin/2006[60]) and considering 1 bar crossing to be $dN_B = 1$, we obtain

$$S_i = K \cdot f(l_i) \cdot \frac{m_G}{SEL} \cdot \int_0^{\infty} \int_{I_C}^{\infty} p_I(I) \cdot p_C(I_C) \cdot dI \cdot dI_C \tag{26}$$

Equation (26) contains three unknowns m_T, K, $f(l_i)$. These parameters are determined from S_i of the comminution equation. However, first the relationship between S_i and B_{ij} must be established.

4.6 Relationship between *S* and *B*

An analysis relating S and B is shown in Appendix D. In brief, we first determined a suitable breakage function to represent probabilities of rupture anywhere along a fibre length (Olson et al./2003[59]). Previous work by others, e.g. Corte et al./1980[80], assumed that fibres shortened into only two parts of varying length. Our analysis has no such restriction. We determined B_{ij} for a rupture at any point by introducing matrix A that links B_{ij} and S_i, giving equation (9) in matrix form as shown below:

$$\frac{dn}{dE} = A \cdot n \qquad \text{where } A = (B - I_n) \cdot S \tag{27}$$

Variable $n(E)$ is a column vector whose entries are the fibre mass fraction in each size interval after the energy input dE. We solved equation (9) by diagonalization of A and introducing U_T as the matrix of the eigenvectors. Assuming the process to be Markovian, we re-expressed the population balance as $n_i(after)=V(E)\cdot n_i(before)$, following the procedure of Berthiaux/2000[84]. We thus decompose V into its characteristic roots, which represent the eigenvalues $exp(-S_i \cdot E)$. From the matrix of the eigenvectors we obtained A, and from equation (27), the breakage function B_{ij}. Further details on this analysis are given in Appendix D.

4.7 Curve -Fitting Procedure

Lastly, we selected an appropriate procedure for regression fitting data in fibre length changes before and after refining to equation (26) to obtain S_i. We accomplished this in using Gauss–Newton algorithm method in two steps.

First we determined the functional form of the parameter $f(l_i)$, assuming it to depend on fibre length alone, and to be independent of m_T and K. This was accomplished by fitting curve shapes of S_i vs. fibre length.

Next, having obtained the form of $f(l_i)$, we determined parameters m_T and K simultaneously by regression fitting to equation (26). This was accomplished by the same regression fitting method.

5 Experimental Program

Our experimental program consisted of analyzing fibre length reductions produced by various refiners. We used Matlab™ software coded to calculate simultaneously the selection and breakage function for different refining conditions. Fibre length distributions before and after refining were measured using a Fibre Quality Analyzer (FQA™). The instrument gives fibre length histograms which contain approximately 150 bins with length increments equal to 0.05 mm. In order to reduce the sampling noise and the large time associated with calculating a 150 x 150 element transition matrix, and within it the *S* and *B* matrix, the measured fibre length distributions were compressed into 20 bins with an increment of 0.25 mm and then normalized. Fibres shorter than 0.5 mm were included in the measured distributions of this study, in contrast to the approach of Olson et al./2003[59]. This may introduce an error because short fibres and fines can be generated by peeling off pieces of fibre wall rather than by fibre shortening. However, in this study all fibres were treated as being a result of fibre shortening. The influence of fines on the overall outcome of the parameter calculation was investigated.

The experimental work was carried out in the steps shown as below:

- Validation of the comminution approach
- Evaluation of data from industrial scale pilot plant trials
- Evaluation of data from laboratory refiners

5.1 Validation of Comminution Approach

The aim of this portion of the experimental work was to validate the comminution approach by a simple case of comminution examined by Berthiaux/2000[84] described in Appendix F. This was accomplished by employing an easily detectable tracer fibre in pulp. The tracer fibre was a laboratory-produced Douglas Fir pulp cooked using the "kraft" process to an H-factor of 1600. The resultant pulp was carefully washed and later classified three times in accordance to TAPPI test method T233 cm-95 with the *Bauer-McNett classifier*. Only the R14 long fibre fraction of the original pulp was retained and further classified to obtain a narrow distribution (3-4 mm) of long fibres as the tracer. As a result of this procedure, we obtained a nearly perfect, defect-free pulp having a narrow length distribution as shown in Figure 8.

Figure 6: Sprout-Waldron LC-Plate (*CEL* = 0.81328 km/rev)

For the validation, a pulp mixture (2% Douglas Fir tracer fibre and 98% White Spruce) was circulated through a single-disc refiner shown in Figure 7. The flow loop consists of two large, 455 liter plastic tanks, a 20 HP centrifugal pump, and a PVC pipe network that circulated the pulp from one tank, through the refiner and into the second tank (or into the

same tank for batch refining). The pulp suspension of 3 % was refined at a target *SEL* of 3 J/m at 600 rpm up to a *SRE* of 240 kWh/t.

Bar Width [mm]	Groove Width [mm]	Groove Depth [mm]	G. Base Radius [°]	Draft Angle [°]
2.9	2.8	2.8	0.5	3

Table 1: Sprout-Waldron Plate Dimensions

Nominal Angle [°]	Cluster Angle [°]	Avg. Int. Angle [°]	Groove Volume [cu. cm/cm]
10	22.5	46.5	0.566

Table 2: Sprout-Waldron Angle Analysis

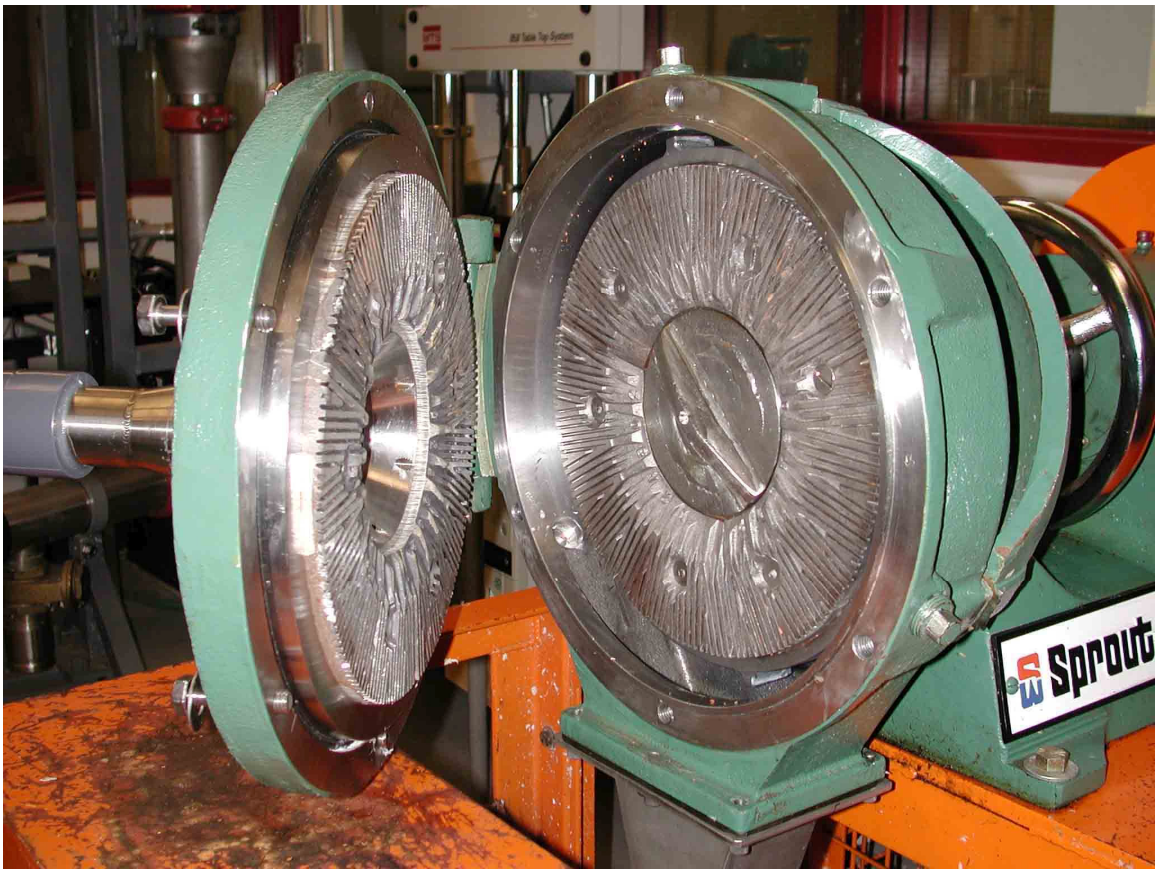

Figure 7: 12” Sprout-Waldron Refiner at UBC (8”inner - and 12”outer diameter)

Pulp samples were obtained at energy increments of 30 kWh/t. From the samples of refined pulp, approximately 100 tracer fibres were collected by pipette under a microscope. The sampling procedure was repeated 30 times in order to obtain a sufficient amount of fibres for measurement of fibre length in the Fibre Quality Analyzer (FQA).

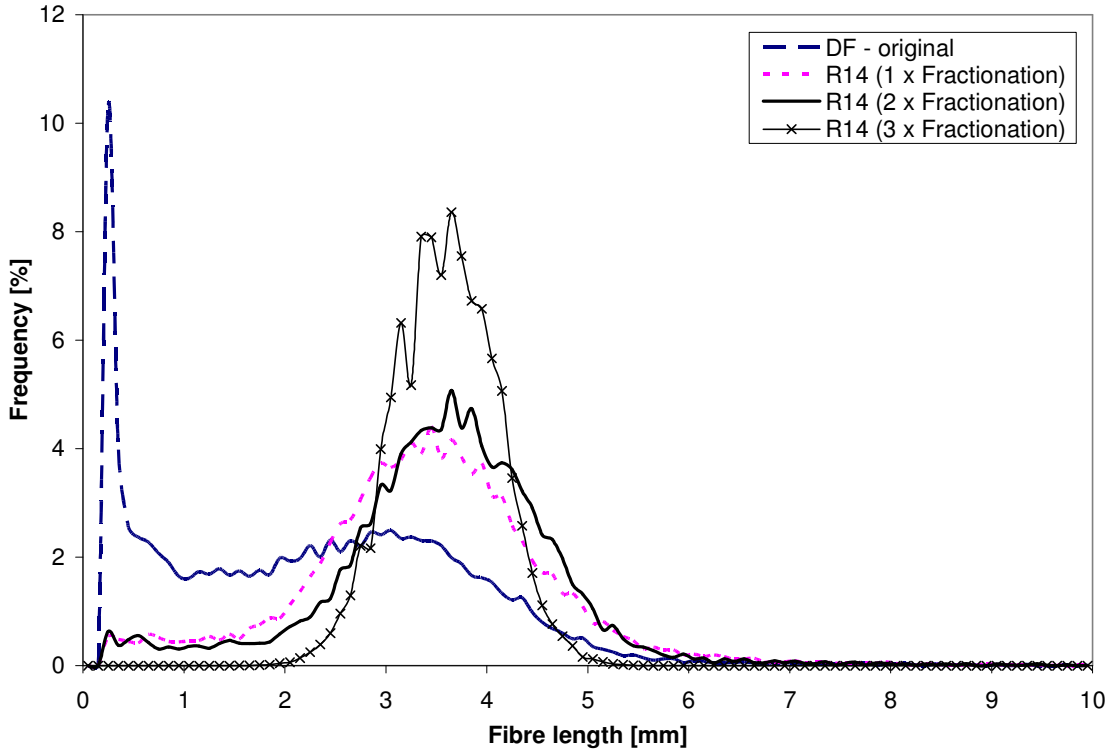

Figure 8: Fibre Length Distribution of tracer fibres (Douglas Fir)

5.2 Pilot-scale Refining Trials

The major portion of the data in this experimental program were supplied by Domtar Inc. and were the same data used by Olson et al./2003[59]. The data were obtained on a 22" Beloit Double Disc pilot refiner and an Escher–Wyss laboratory refiner. The trials examined five different plate patterns. For each plate pattern, a range of energies and intensities were explored. Table 3 summarizes the experimental conditions of the various

refiners. The reported power is the net power, P_{net}, which is the total power less the no-load power. The consistencies are nominal values. The rotational speed for the double disc refiner (22" Beloit Double Disc) is 900 rpm and for the Escher-Wyss refiner is 1000 rpm. The plate dimensions used in this study are summarized in Table 4.

Trial	Refiner	Plate	Consistency [%]	$\dot{m}$ [t/d]	P_{net} [kW]	*SEL* [J/m]
A	22" Beloit Double Disc	1	2.84	14	65	3.25
B			4.55	14	64	3.20
C			1.55	8	34	1.70
D			2.48	7	34	1.70
E			4.22	7	34	1.70
F		2	4.19	9	64	2.67
G			2.54	6	26	1.08
H			4.52	6	26	1.08
I		3	2.70	7	33	0.14
J			4.40	7	34	0.14
K			2.56	4	16	0.07
L		4	4.51	12	55	7.86
M			3.15	13	56	8.00
N	Escher-Wyss	5	1.50	-	0.7	1.50
O			3.00	-	1.4	3.00
P			4.00	-	2.3	5.00
Q			3.00	-	2.3	5.00

Table 3: Summary of experimental trials from Olson et al./[59].

Plate	Bar Width [mm]	Groove Width [mm]	Groove Depth [mm]	Bar angle [°]	*CEL* [km/s]
1	3.0	3.0	4.0	17.3	20.05
2	2.5	2.5	5.0	21.5	24.1
3	1.0	2.5	1.0	21.25S, -26.5R	233.2
4	3.0	8.0	4.0	21.25	7.0
5	6.0	12.0	8.0	16.0	0.521

Table 4: Summary of refiner plate geometries.

In addition to measurements of fibre length, some key changes in paper properties resulting from refining were measured, namely, sheet density, burst index, tear index,

breaking length, tensile index, as well as *T.E.A.* These were measured according to the appropriate TAPPI standard.

5.3 Escher-Wyss Heterogeneity Trial

Another set of tests was carried on the laboratory Escher-Wyss laboratory refiner in the Vancouver Laboratory of FPInnovations (Paprican) with assistance of Phil Allen of FPInnovations. This refiner has a rather coarse bar pattern with pulp circulating many times through the working zone.

The following trial plan was employed:

Trial #	C_F [%]	*SEL* [J/m]	Energy Increments [kWh/t]
1	2	4	30/60/90/120
2	3	4	6/12/18/24/30/60/90/120
2	4	4	30/60/90/120
4	2	2	30/60/90/120

Table 5: Escher-Wyss trial conditions

The Escher-Wyss refiner was set to 1000 rpm. The plate patterns used in this study were the same as for Plate 5 in Table 4.

5.4 Conflo Refining Trial

In addition to the above tests, a series of refiner trials were carried out using a industrial-size Conflo JC-00 conical refiner (angle of conical refiner is 20°) at various speeds. The tests were carried out with the assistance of Bill Francis and Norman Roberts of FPInnovations. The entry and exit diameters of the rotor of this refiner were 192 mm and 380 mm. The refiner plate geometry data are shown in Table 6.

Bar Width [mm]	Groove Width [mm]	Groove Depth [mm]	Bar angle [°]
5.65R, 5.67 S	6.79R, 7.25S	8.88R, 9.37S	18

Table 6: Conflo JC-00 refiner plate geometry.

The resulting *CEL* was calculated to be 1,009 m/rev. The pulp in use was a BC Interior SPF with 50% Lodgepole Pine, 40% White Spruce, 6% Sub-Alpine Fir and 4% other species. Table 7 summarizes the trial conditions. The target *SEL* was 4 J/m at a suspension consistency of 1%.

Run #	ω [rpm]	Q [l/min]	P_{net} [kW]	*SEL* [J/m]	*SRE* [kWh/t]
1	148	256	9.6	3.88	63
2	147	499	10.2	4.10	34
3	148	1019	9.7	3.88	16
4	996	262	67.9	4.05	431
5	996	527	68.0	4.06	215
6	996	1018	67.8	4.04	111
7	510	254	33.4	3.89	219
8	510	522	33.7	3.93	108
9	510	994	33.5	3.90	56
10	242	249	17.0	4.18	114
11	738	748	51.2	4.13	114
12	1095	1087	76.1	4.14	117

Table 7: Conflo JC-00 trial conditions

6 Results and Discussion

6.1 Validation of Comminution Approach

As described earlier, some preliminary tests were carried out in the Sprout Waldron refiner by placing lab-cooked tracer fibres in a standard pulp. After refining, tracer fibres were sampled from the refined pulp and examined visually for physical deformations indicative of impacts. A visual separation of tracer fibres from the commercial chemical pulp was possible due to the colour difference. The tracer fibres were not bleached and therefore appeared brown whereas the White Spruce fibres were bleached and white in appearance. As shown in Figure 9, some fibres showed no evidence at all of having been impacted while others showed external fibrillation, yet others appeared straightened. Some cutting was also evident as shown in Figure 9.

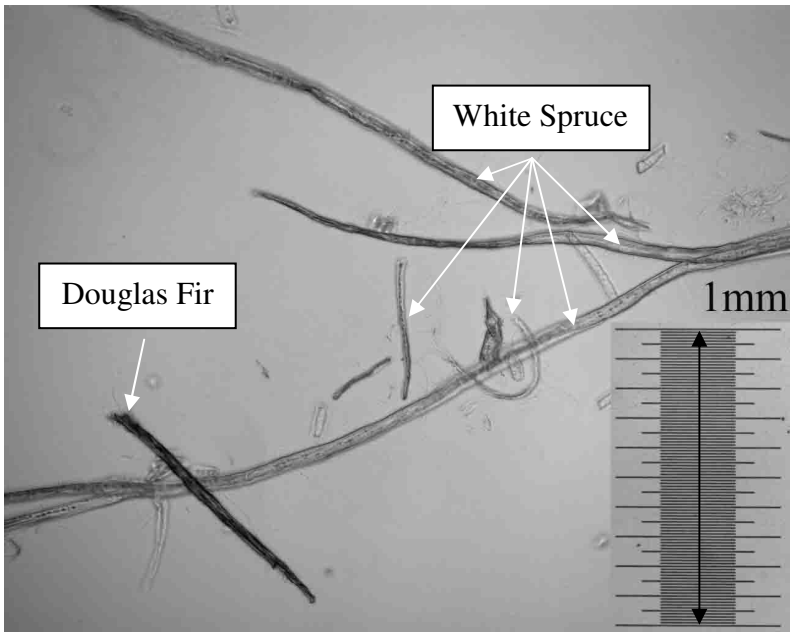

Figure 9: Refined Douglas Fir (dark brown) and White Spruce fibres using the 12" Sprout-Waldron refiner

As expected due to the high *SEL* of 3 J/m, the number of short fibres increased and the number of long decreased. Based on the resultant fibre length distribution, a simple calculation of the selection function probability for the longest fibre fraction, i.e. 4.3 mm long fibres, was performed using following relationship:

$$n_{after,longest} = \left[\exp\left(-S_{longest} \cdot SRE\right)\right] \cdot n_{before,longest} \tag{28}$$

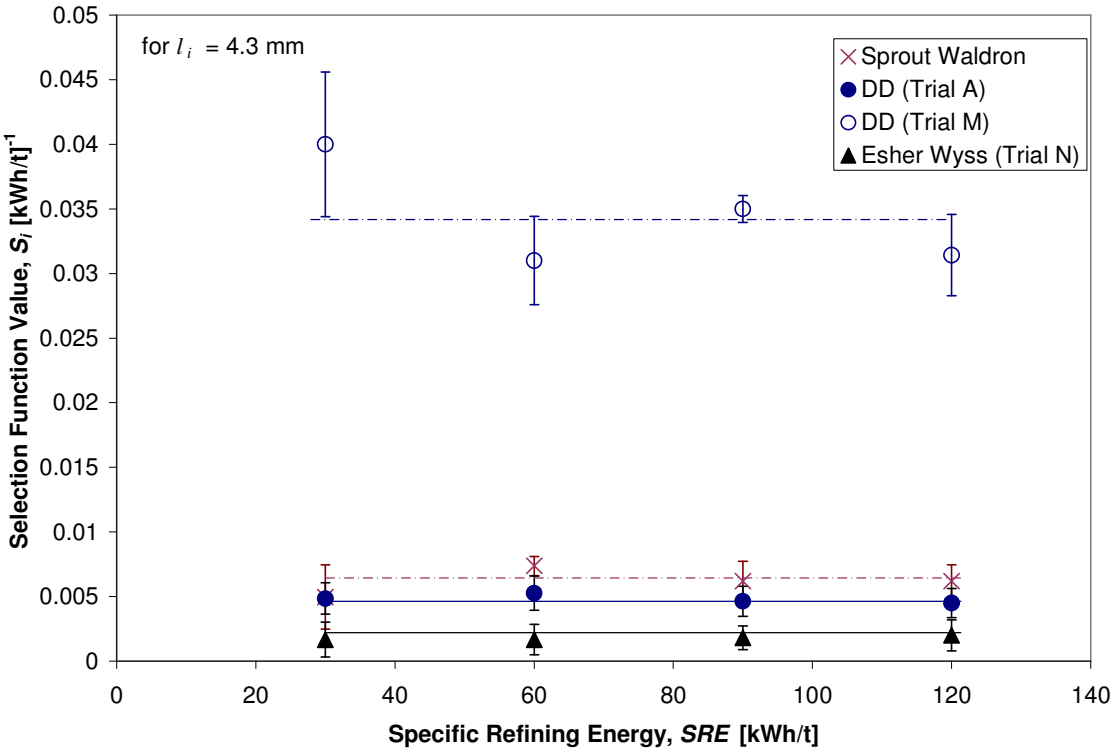

Figure 10: Comparison of the selection function probability, S_i, for 4.3 mm long fibres (White Spruce) for various trial conditions and refiners

The result was compared to values obtained with the double disc and Escher-Wyss refiner trials. As seen in Figure 10, for energies greater than 40 kWh/t the selection function was approximately independent of specific energy for the single disc, double disc and Escher Wyss refiners tested, as found by Olson et al./2003[[59]]). This energy independence of selection function allows comparison of selection functions between refiners operating at

different energies. It also validates the application of our approach to calculate S_i and B_{ij} using Markov chains. However, once again, the new approach is only possible as long as there is a measurable amount of cutting.

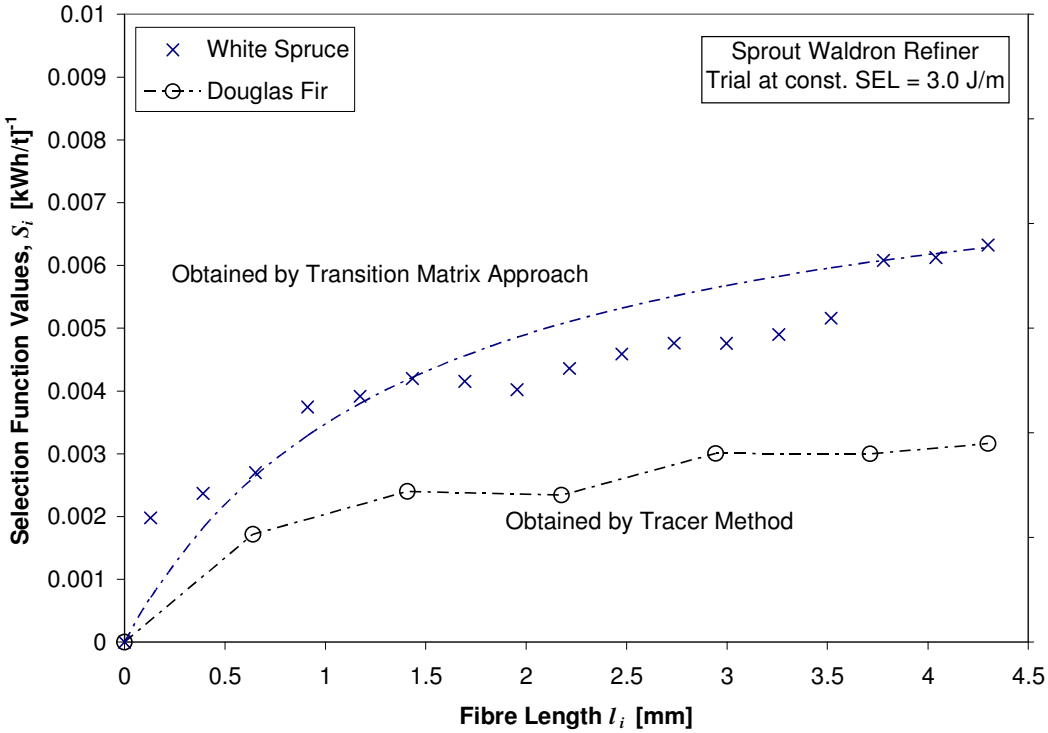

Figure 11: Selection function curve for Douglas Fir and White Spruce fibre fractions after refining at *SEL = 3.0 J/m*

The curves in Figure 11 show that the selection function dependence on fibre length for the two cases follows a similar trend but differs in magnitude. This difference may be due to several possible factors. By our estimate, the Douglas Fir tracer fibre is about 25% stronger than the White Spruce pulp (Ellis and Rudie/1991[85]), and likely even stronger because it is an undamaged lab-cooked fibre as opposed to the commercially produced White Spruce. Thus, it is less likely to rupture when captured, thereby giving smaller S_i values as shown in Figure 11. Yet another factor is the assumption of an increment of energy being 30kWh/t. This is 1/4 of the total energy applied in this trial, and is therefore

very large as an incremental energy. In contrast, the incremental energy in the matrix-based estimate is the much smaller energy of an individual bar crossing. Nevertheless, the two curves show a similar trend in that fibre shortening increases sharply with increasing fibre length for small fibres, then increases at a smaller rate for longer fibre lengths.

6.2 Selection and Breakage Functions

The statistical significance of the measured differences among the trials were evaluated by Student's t-Test. Differences emanating from the transition matrix calculation were considered statistically significant if the probability associated with a Student's t-Test was smaller than 0.65 (A value of 0 would mean that the fibres have been cut severely whereas a value of 1 signifies no cutting, meaning a change in arithmetic fibre length less than 15%.)

6.2.1 Selection Function

We now examine the relationships between selection function and some refining variables at observed length changes. Figure 12 shows the selection function dependence on fibre length for various *SEL*'s on the Escher Wyss lab refiner using the same refining plate. The tests were conducted by varying the applied power and pulp consistency. It is apparent that the selection function increases with fibre length, but tends to plateau at longer fibre lengths as found in the tracer fibre studies (Figure 11). For a given fibre length, the selection function increases with increasing *SEL*, meaning increasing power because the *CEL* was not changed.

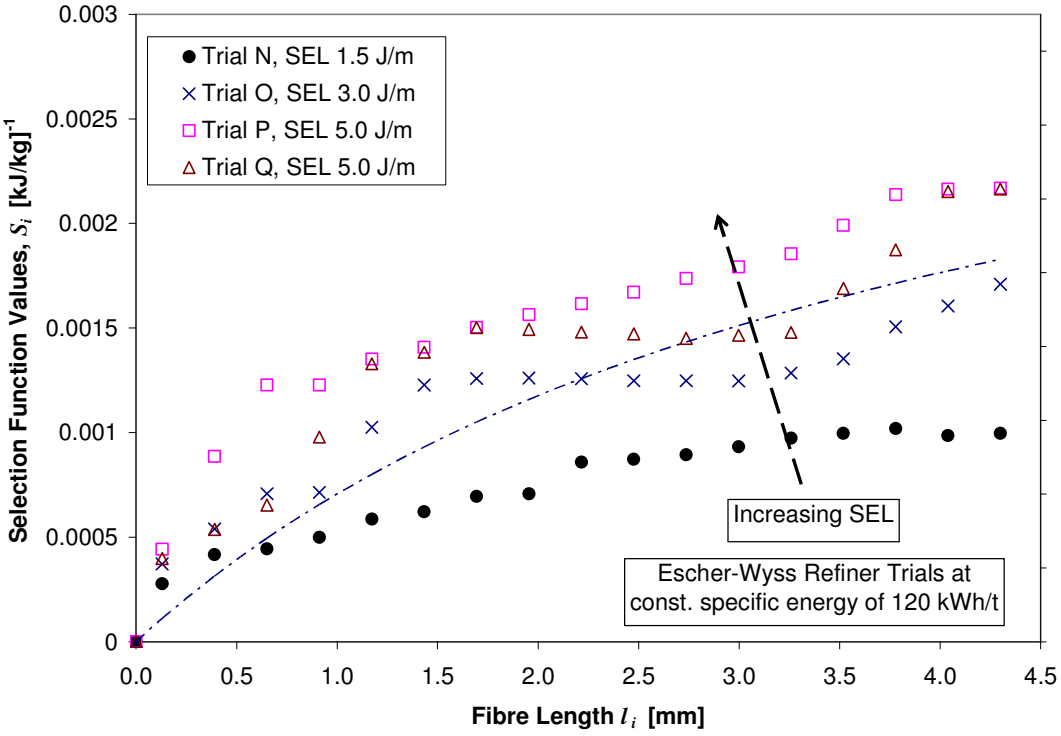

Figure 12: The experimentally determined selection function for the Escher–Wyss refiner trials using a single refiner plate for increasing *SEL*.

The effect of *SEL* on selection function is further illustrated in Figure 13 for fibres of 3.3 mm length from all of the tests. The probability of a fibre being selected for cutting clearly increases with *SEL*, moderately up to *SEL* = 2 J/m, more in the *SEL* 3-5 J/m range, and then greatly at the *SEL* = 8 J/m range. Thus, fibre shortening clearly depends on intensity as well as probability of capture.

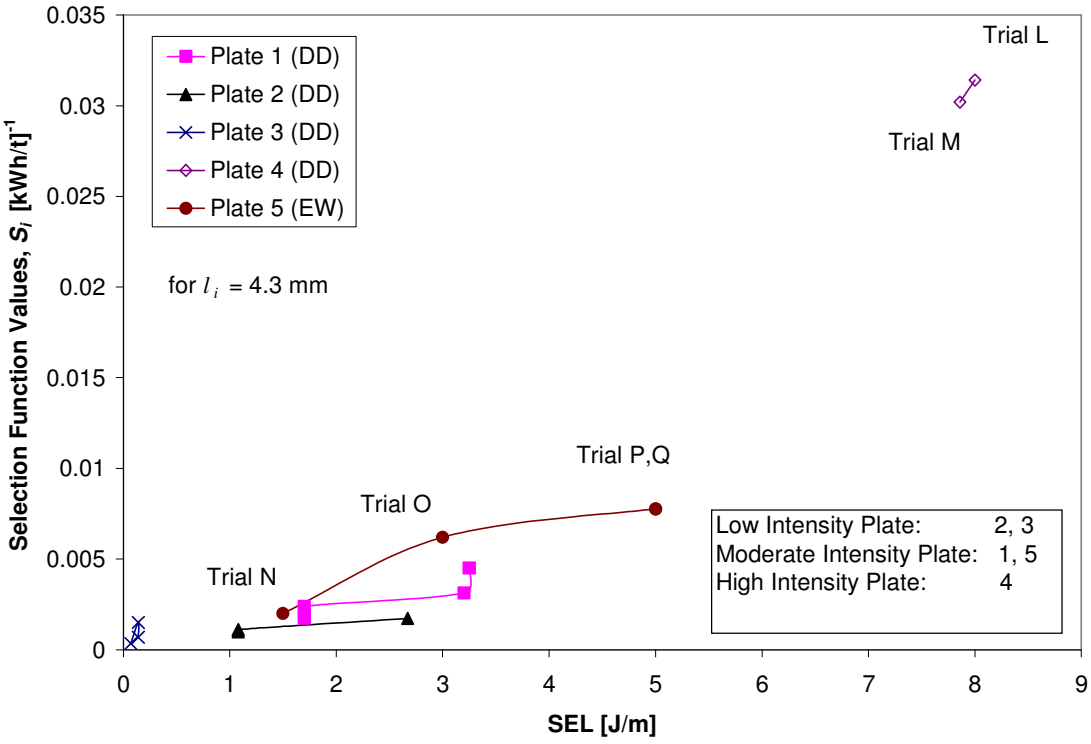

Figure 13: Selection function values for 4.3 mm long fibres for all 15 trials

The selection function decreases with consistency as shown in Figure 14 for a fibre length of 4.3 mm in a double disc refiner at a constant rotational speed with the same plate pattern. These data also show that larger consistency gives a smaller probability of fibre capture. In addition, a strong dependency on Specific Edge Load was evident, similar to the laboratory Escher Wyss results. The likely explanation for this decrease in selection function with increasing consistency is the decreasing mobility of fibres relative to one another. In the case of decreasing mobility, long fibres are not preferentially captured relative to short fibres. Consequently the 4.3 mm fibres in a high consistency suspension have a lower value of selection function.

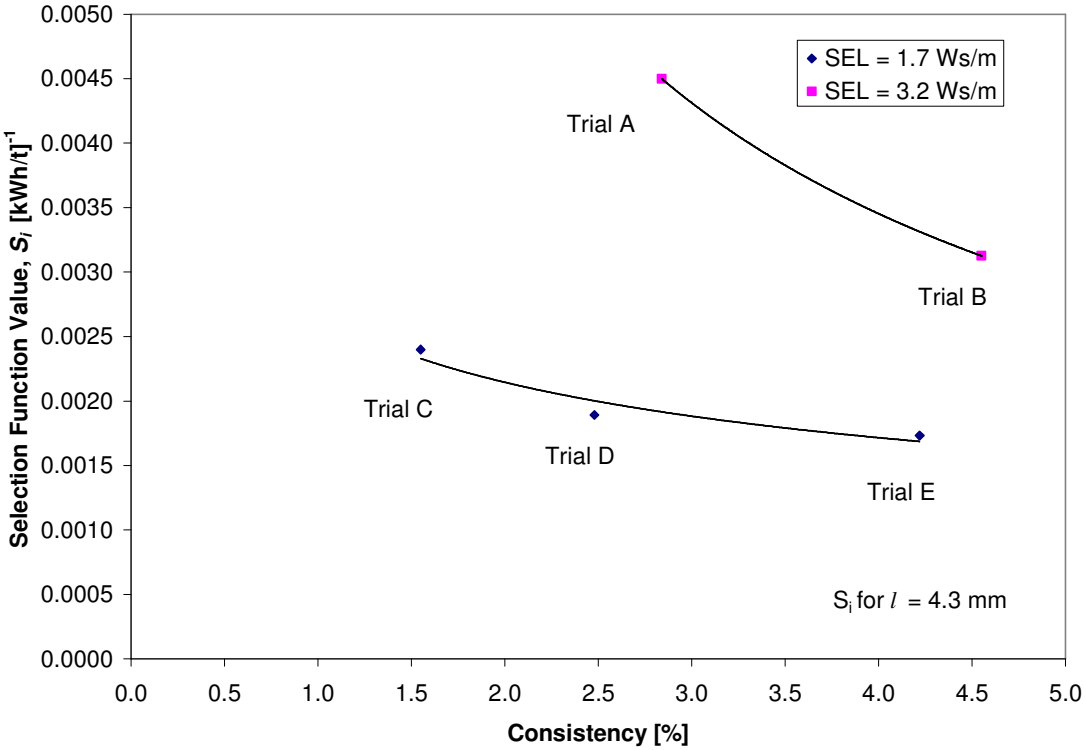

Figure 14: Selection function dependency on Consistency for the same plate pattern on a Double Disc refiner (Trial A-E) for fibre length of 4.3 mm

6.2.2 Breakage Function

As described earlier, unlike previous approaches, this study did not assume a form of the breakage function. By determining the breakage functions, some insight can be gained on the position along fibre lengths where rupture occurs. This is illustrated in Figure 15. For fibres less than 3 mm in length, there is an increasing probability that daughter fibres will be similar in length to the length of original fibres. Clearly in this length range there is no maximum. However, above 3 mm, there is a maximum at about 0.75, meaning that longer fibres are cut to about ¾ of their original length. This trend was found in all the cases tested. In summary Figure 15 suggests that refiners preferentially cut near the ends of fibres.

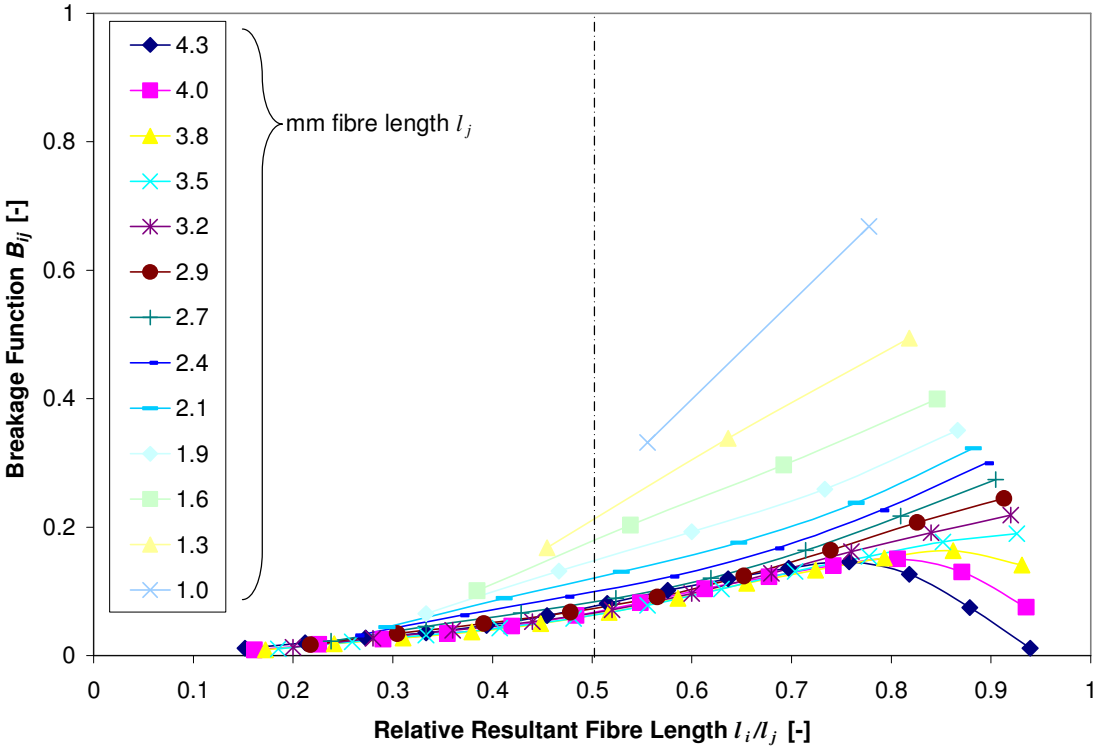

Figure 15: Breakage probability of White Spruce fibres during trial E.

6.3 Determining Parameters Affecting Selection Function

We now consider the variables which govern the selection function in order to obtain the key parameters that describe heterogeneity of refining action. We do so from equation (26), which is reproduced below:

$$S_i = K \cdot f(l_i) \cdot \frac{m_G}{SEL} \cdot \int_0^{\infty} \int_{I_C}^{\infty} p_I(I) \cdot p_C(I_C) \cdot dI \cdot dI_C \qquad (26)$$

There are three unknowns in this equation: two, K and $f(l_i)$ describe the probability of impact, and the third unknown, m_T, the mass in the gap, gives the average intensity I_A where $I_A = SEL / m_T$.

6.3.1 Determining $f(l_i)$

As described earlier, the functional form of the length dependence of capture factor, $f(l_i)$, can be determined from the shapes of curves of the type, as shown in Figure 12 (dotted line). This was accomplished by fitting various length functions to the data by regression analyses. This procedure assumed that K and m_T did not affect the form of the function.

The form of $f(l_i)$ examined were once reported by earlier workers, e.g. effect of groove depth (Kerekes1990/[55]) and consistency (Batchelor and Ludin/2006[60]). The various forms examined are summarized in Appendix G.

The best fit obtained was of the form:

$$f(l_i) = \frac{l_i}{l_i + 0.5 \cdot D} \tag{29}$$

6.3.2 Determination of K and m_T

The parameters K and m_T in equation (26) were determined by regression fitting the data obtained for S_i as function of l_i to equation (30) below. In this equation K is a unknown constant and m_T appears in the average intensity I_A ($I_A = SEL / m_T$) in the integrals.

$$S_i = K \cdot \frac{l_i}{l_i + 0.5 \cdot D} \cdot \frac{m_G}{SEL} \cdot \int_0^{\infty} \int_{I_C}^{\infty} p_I(I) \cdot p_C(I_C) \cdot dI \cdot dI_C \tag{30}$$

The results from the regressions are shown in Table 8. A representative energy input of SRE = 120 kWh/t was arbitrary chosen for the regression. The average number of impacts, N_A, experienced by fibres was calculated from $N_A = m_T/m_G \cdot N_B$ (equation (17)).

Trial	Plate	Refiner	Plate	Intensity (SEL)	SRE [kJ/kg]	SEL [kJ/m]	m_G [kg/m]	C_F [%]	K [-]	m_T [kg/m]	m_T/m_G [-]	I_A [kJ/kg]	N_A [-]
A					450.0	0.00324	6.82E-04	2.84	0.062	1.66E-04	0.244	19.5	23
B					432.0	0.00319	1.09E-03	4.55	0.051	2.06E-04	0.189	15.5	28
C	1		1	moderate	414.0	0.00170	3.72E-04	1.55	0.040	9.63E-05	0.259	17.7	23
D					435.6	0.00171	5.95E-04	2.48	0.015	8.49E-05	0.143	20.1	22
E					439.2	0.00171	1.01E-03	4.22	0.012	1.00E-04	0.099	17.0	26
F					414.0	0.00267	1.05E-03	4.19	0.023	1.76E-04	0.168	15.2	27
G	2	DD	2	low	414.0	0.00108	6.35E-04	2.54	0.007	6.23E-05	0.098	17.3	24
H					421.2	0.00108	1.13E-03	4.52	0.005	6.58E-05	0.058	16.4	26
I					327.6	0.00014	1.35E-04	2.70	0.069	3.60E-05	0.267	3.9	84
J	3		3	ultra-low	446.4	0.00014	2.20E-04	4.40	0.011	6.37E-05	0.289	2.2	203
K					424.8	0.00007	1.28E-04	2.56	0.004	2.82E-05	0.220	2.5	171
L	4		4	highest	432.0	0.00786	2.89E-03	4.51	0.068	1.98E-04	0.069	39.6	11
M					414.0	0.00800	2.02E-03	3.15	0.115	2.31E-04	0.114	34.7	12
N					432.4	0.00150	2.88E-03	1.50	0.003	6.62E-05	0.023	22.7	19
O	5	EW	5	moderate	429.1	0.00300	5.76E-03	3.00	0.022	1.23E-04	0.021	24.3	18
P					428.0	0.00500	7.68E-03	4.00	0.008	1.66E-04	0.022	30.1	14
Q					427.0	0.00500	9.60E-03	3.00	0.007	2.05E-04	0.021	24.4	18

Table 8: Comparison of obtained values for K, m_T , I_A and N_A for a representative specific energy input of 120 kWh/t (all are converted into SI-units)

6.4 Discussion of Predicted Probabilities and Intensities

We now examine and compare the probabilities of impacts (capture) and the average intensity of impacts on fibres obtained from the regression analysis.

6.4.1 Probability of Impact

Recalling from equation (29) that the factor of capture of a fibre of length l_i at a single bar crossing is given by $F_{Ci} = K / (l_i + 0.5 \cdot D)$, we now examine factors which affect this probability. As expected, F_{Ci} increases with decreasing groove depth, as shown in Figure 16. This occurs because the fibre capture sweep zone by a bar edge occupies a larger fraction of the total groove depth. It is further evident in Figure 16 that F_{Ci} increases with increasing groove width up to about 5 mm, and then decreases beyond this level. The likely explanation for increasing F_{Ci} is that a wider groove gives a longer sweep zone which enables more fibre capture. However, this increase has a limit which is likely the capacity of the gap to hold fibre, or the maximum mass of fibres which a bar edge can

capture. Such a limit was observed by Smith/1922[24] in drawing a bar through an infinite reservoir of pulp. For example, he found that at 3% consistency pulp, a bar captured fibres up to a level of about 0.001 kg/m. We may note here that a sweep length of 5 mm over a depth equal to a fibre length of 2.5 mm contains about 0.0004 kg/m pulp. For a sweep length of 12 mm, this would be about 0.001 kg/m, which is about the limit found by Smith/1922[24].

The probability of fibre impact also depends on flow conditions in a refiner. This is shown in Figure 17. As radial flow velocity increases, the probability of fibre impact increases for an average constant tangential velocity of 26.3 m/s (in case of the double disc refiner) or 6.1 m/s (Escher Wyss laboratory refiner) respectively.

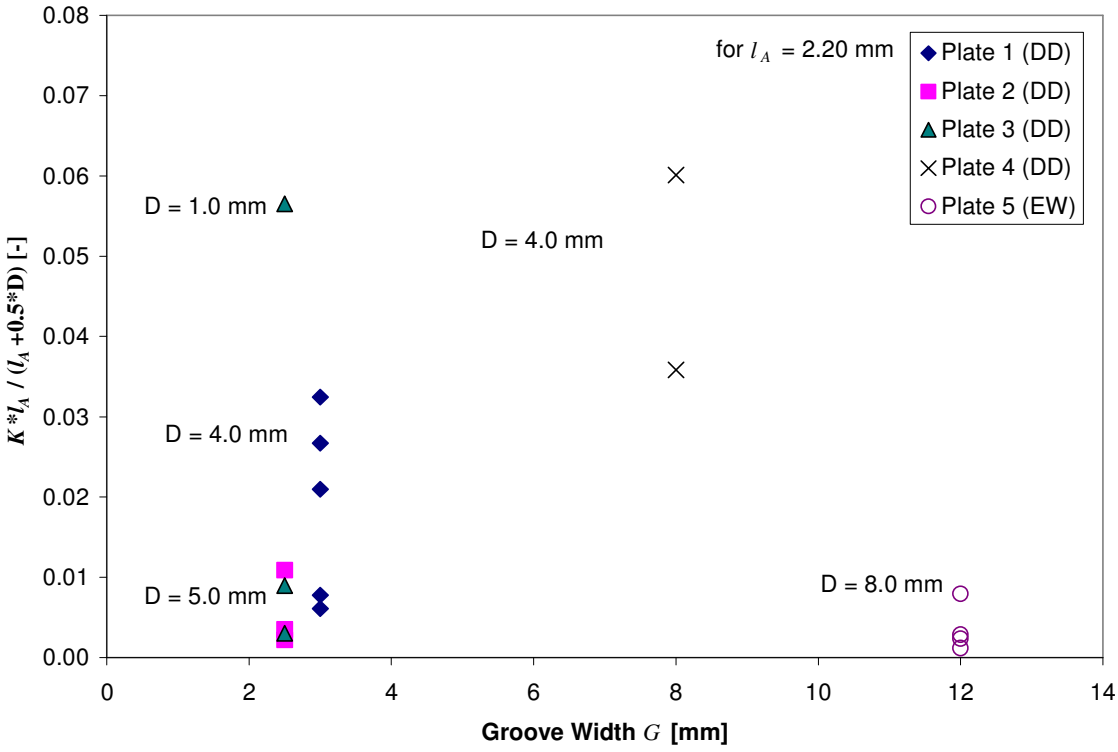

Figure 16: Probability of capture for average fibre length l_A during one bar crossing for various plate geometries

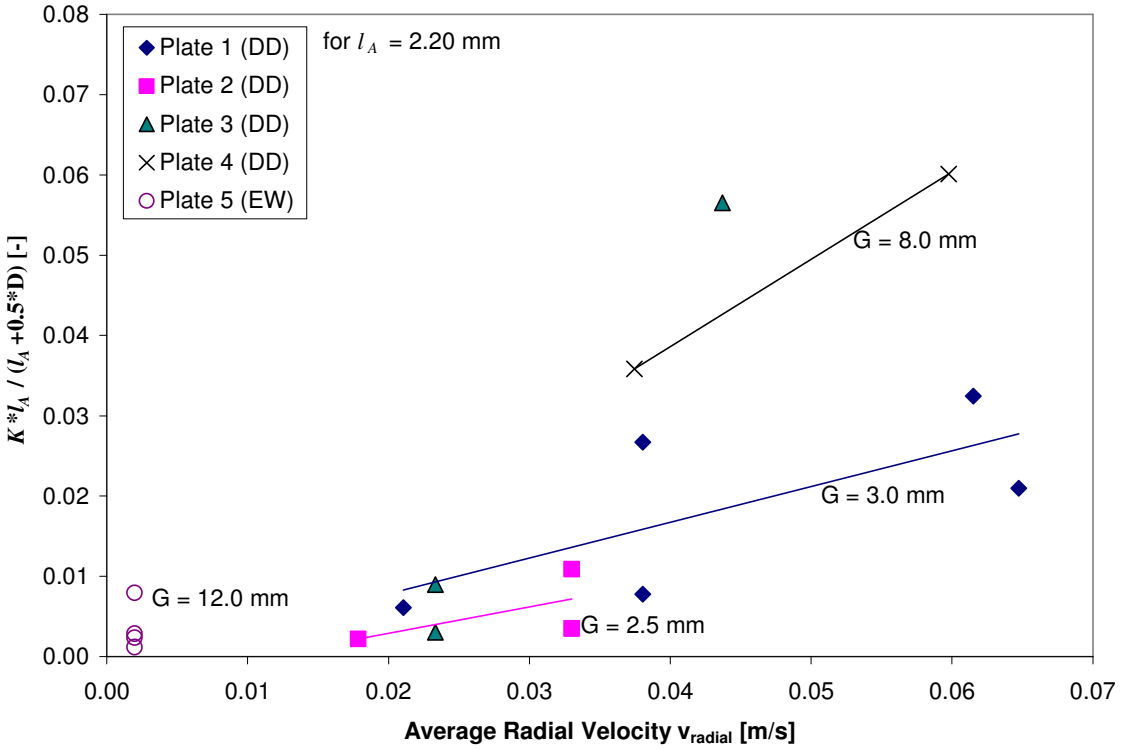

Figure 17: Capture probability for average fibre length l_A during one bar crossing for various flow conditions

6.4.2 Intensity of Impacts

Values for the average intensity of impact I_A are shown in Table 8. For a given *SEL*, I_A depends on m_T. The values of m_T from the regression vary from $2.3 \cdot 10^{-4}$ kg/m to $2.83 \cdot 10^{-5}$ kg/m, a range which appears reasonable. For example, assuming a consistency for the compressed fibre mat in a refiner gap to be of 30%, a gap of size 0.15mm and 3 mm bar width would hold about 10^{-4} kg/m of fibres.

The values of m_T obtained give levels of I_A in Table 8 from 2.2kJ/kg to 39.6 kJ/kg. This range is also reasonable. Evidence of this is shown by fibre shortening in Figure 18, where fibre length is relatively unaffected up to an average intensity of about 20 kJ/kg, then diminishes significantly as intensity increases beyond this value.

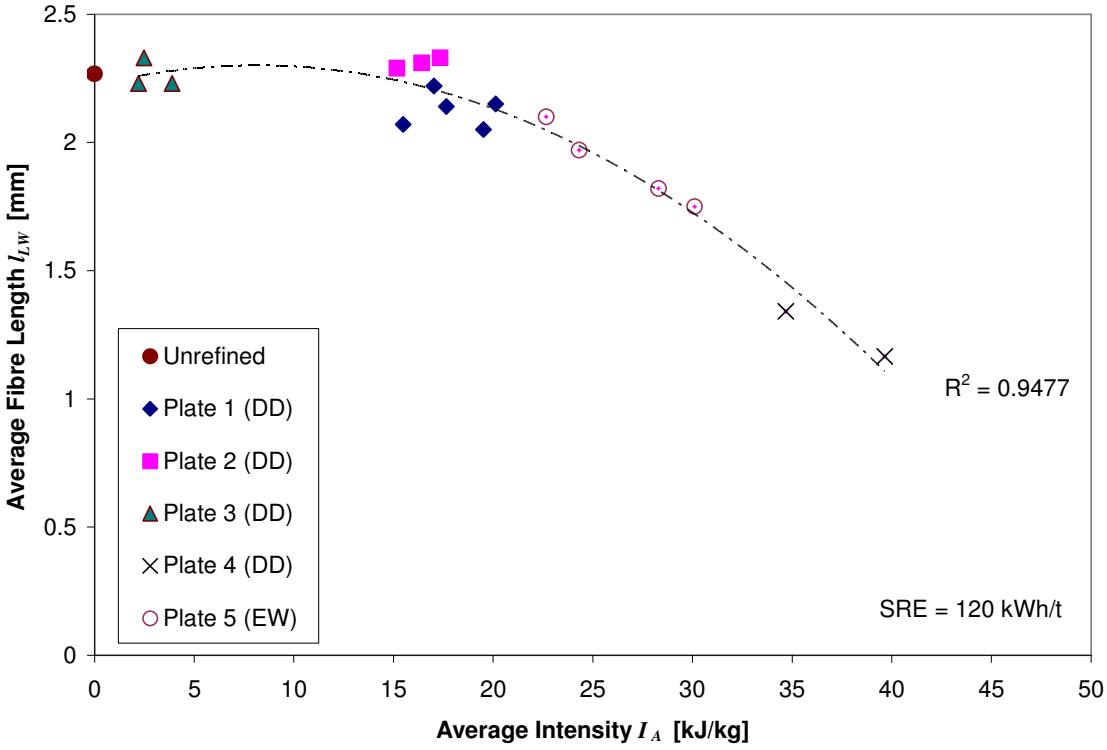

Figure 18: Fibre-length-reduction characterization as function of intensity.

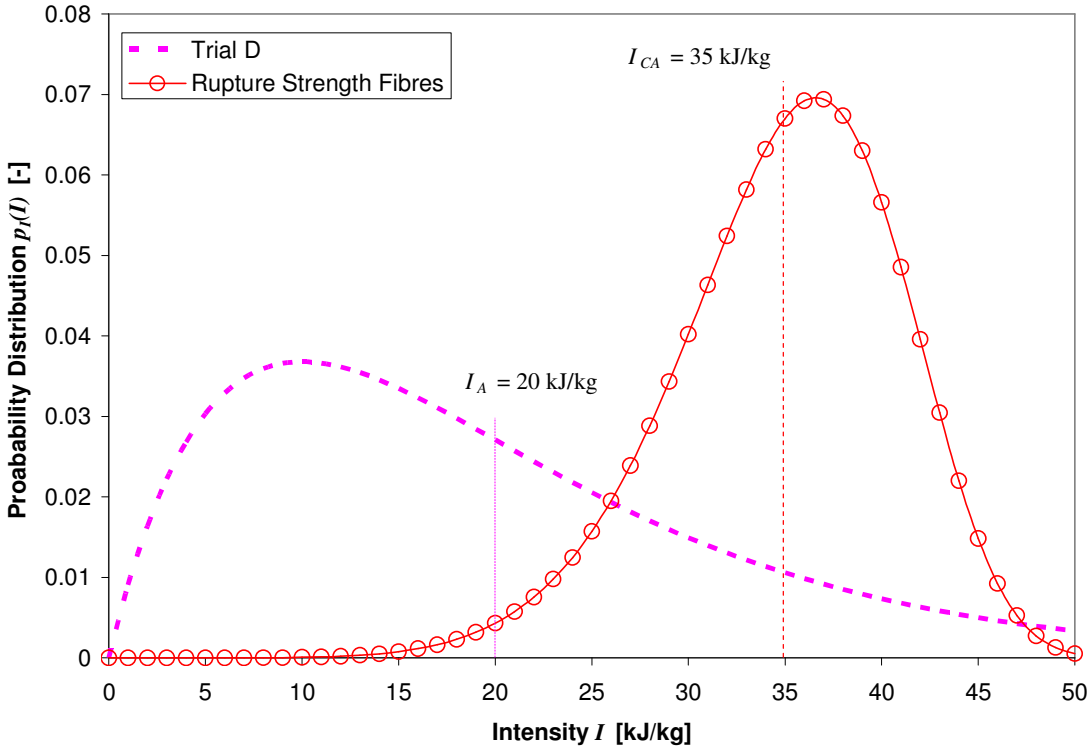

Figure 19: Actual intensity distribution vs. the distribution of rupture strength, I_C.

The estimated fibre rupture strength is 35 kJ/kg, meaning that values in the high end of the distribution about 20 kJ/kg exceed this value. This takes place as shown in Figure 19.

6.5 Comparisons to Previous Studies

6.5.1 Intensities

We now compare findings of this study to other relevant published work. Leider and Nissan/1977[36] and Kerekes/1990[55] predicted intensities by dividing the specific energy by the estimated number of impacts on pulp fibres. Their predicted intensities are compared to values from this study in Figure 20.

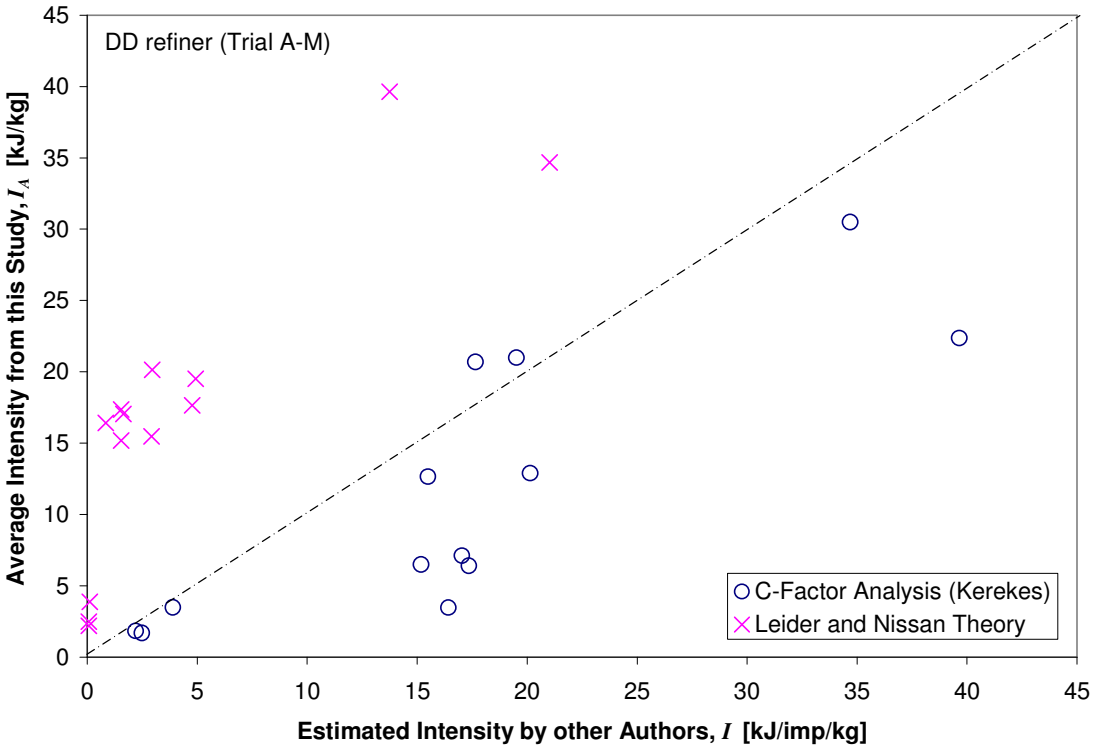

Figure 20: Comparisons of Average Intensity I_A to intensity levels calculated based on previous studies by Leider and Nissan/1977[36] and Kerekes/1990[55].

Clearly the C-Factor predicts larger values then those of this study whereas Leider and Nissan/1977[36] predict smaller values. Thus, the results of this study fall between the values of these earlier studies. Leider and Nissan predict low intensities because they estimate many more impacts than does the C-Factor. They assumed that the number of impacts per fibre per bar crossing is proportional to the ratio of cross-sectional area of a fibre to the cross-sectional area of a groove as well as to the rotational speed. On the other hand, Kerekes' C-Factor assumed the probability of impact to depend upon the ratio l_A / $(l_A + D)$ and suspension consistency, justifying these assumptions by showing that they led to logical outcomes in limiting cases.

6.5.2 Probabilities of Impacts in Compression Refining

In recent work, Goosen et al./2007[86] showed that for compression refining, the development of tensile strength in paper was strongly linked to the probability that fibres experience one impact (loading cycle). This observation suggested that the role of multiple loading cycles in refining was to ensure that many fibres experienced at least one impact, as opposed to the conventional view that the purpose of multiple loading cycles was to introduce fatigue weakening. By a simple statistical model, Goosen et al./2007[86] showed that increase in tensile strength $R(N_C)$ was related to the cumulative probability of an impact, P, over N_C cycles.

$$R(N_C) = 1 - (1 - P)^{N_C} \tag{31}$$

We tested this relationship on the EW refiner by obtaining the tensile strength for given numbers of bar crossings N_B (in place of N_C), as shown in Table 9 and plotted in Figure 21. By regression fitting to equation (31) to these data, we obtained the probability P that gave the best fit.

C_F [%]	*SEL* [J/m]		*SRE* [kWh/t] 6	12	18	24	30	60	90	120
2	2	N_B [-]					207	415	622	829
		BL [km]					4.553	6.105	7.152	7.604
2	4	N_B [-]					104	207	311	415
		BL [km]					4.878	5.918	7.058	7.672
3	4	N_B [-]	31	62	93	124	156	311	467	622
		BL [km]	3.396	3.869	4.154	4.376	4.646	5.65	6.138	7.151
4	4	N_B [-]					207	415	622	829
		BL [km]					4.454	5.805	6.697	6.814

Table 9: Escher-Wyss trails including calculated number of bar crossings, N_B and breaking length, *BL*

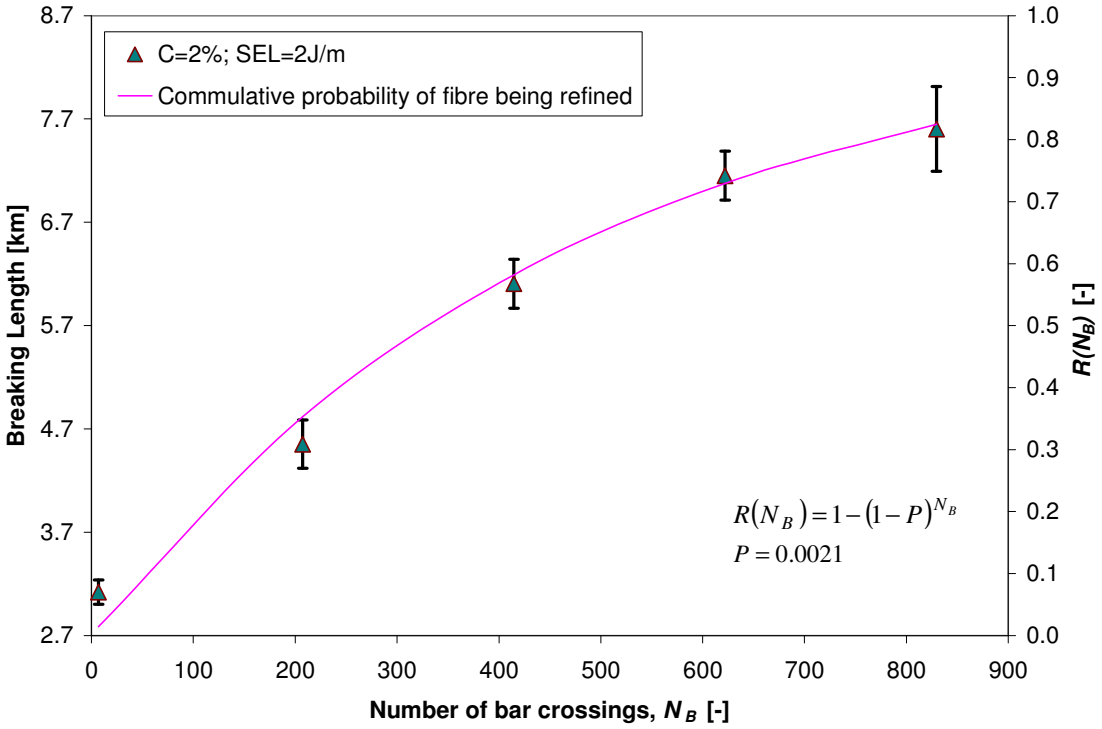

Figure 21: Tensile strength plotted against cumulative probability for $P = 0.0021$.

The result for a consistency of 2% and an *SEL* = 2 J/m was $P = 0.0021$. This value is close to the value of $F_{Ci} = 0.0023$ obtained from $K \cdot l_A / (l_A + 0.5 \cdot D)$ in Table 8 for the Escher Wyss trials of the previous section. For all four combinations of consistency and *SEL*, probability *P* ranged from 0.0019 to 0.0045. Though not conclusive, this finding seems to confirm that probabilities of impacts found in this study are sound, as can be

seen in Figure 22. It further suggests that the role of multiple loading cycles in refining is to ensure that many fibres see at least one impact as opposed to introducing fatigue weakening, in short, that the role of multiple loading cycles is to reduce heterogeneity.

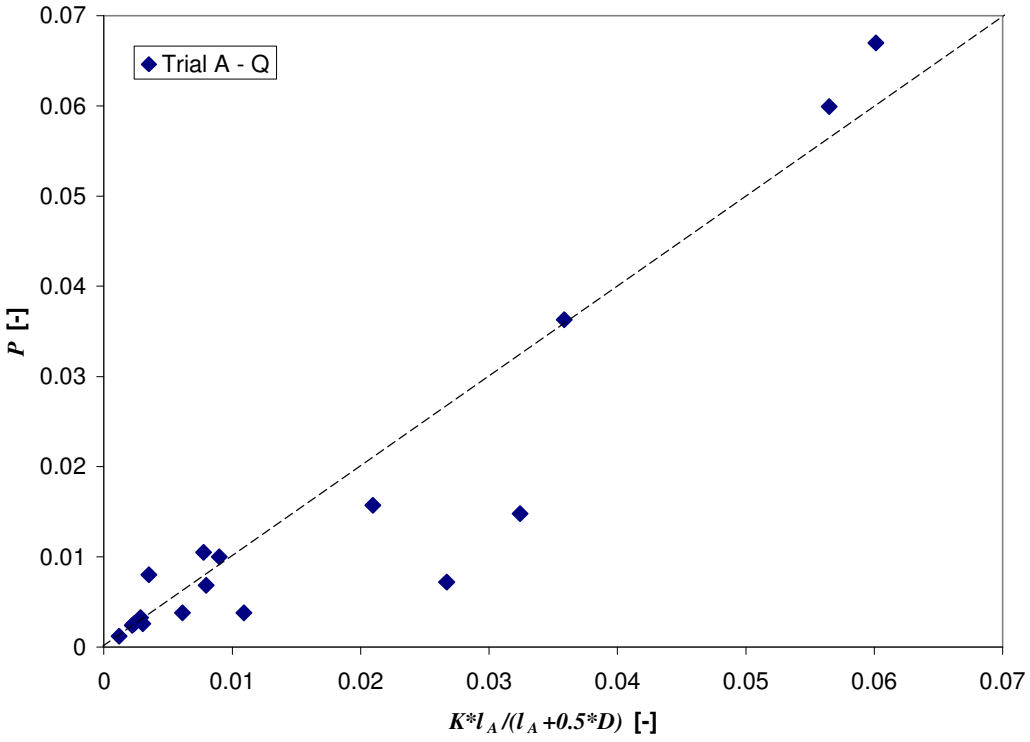

Figure 22: Comparison of $K \cdot l_A / (l_A + 0.5 \cdot D)$ and P for Trials A - Q

6.6 Homogeneity Index

We now address the question of defining a useful parameter to represent heterogeneity. For convenience, in order to have a larger value represent a better result, we will define heterogeneity in terms of its inverse – homogeneity. A "Homogeneity Index" may be used to characterize operating refiners. From an industrial standpoint, it is desirable to have a single number index. However, in reality this is difficult. Homogeneity is affected by the number and intensity of impacts as well as by the distribution of each of these variables. Moreover, each of these has subset of additional factors. All this gives rise to

many possible combinations of parameters that could be employed to define a homogeneity index, *H*. Somewhat arbitrarily, we choose the following: the product of the number of impacts on fibres of average length and the fraction of intensities within +/- 2 kJ/kg of the average intensity, divided by the specific refining energy, *SRE*. This can be expressed as:

$$H = \frac{K \cdot \frac{l_A}{l_A + 0.5 \cdot D} \cdot N_B \cdot P\left(I_A \pm 2kJ/kg\right) \cdot I_A}{SRE} \tag{32}$$

Values of *H* for our tests are summarized in Table 10 along with the key refiner variables and computed parameters.

Trial	Plate	Refiner	Plate	Intensity (SEL)	SRE [kJ/kg]	SEL [kJ/m]	m_G [kg/m]	C_F [%]	m_T [kg/m]	N_B [-]	I_A [kJ/kg]	N_A [-]	H [-]
A	1	DD	1	moderate	450.0	0.00324	6.82E-04	2.84	1.66E-04	95	19.5	23	0.015
B					432.0	0.00319	1.09E-03	4.55	2.06E-04	148	15.5	28	0.020
C					414.0	0.00170	3.72E-04	1.55	9.63E-05	91	17.7	23	0.010
D					435.6	0.00171	5.95E-04	2.48	8.49E-05	152	20.1	22	0.006
E					439.2	0.00171	1.01E-03	4.22	1.00E-04	260	17.0	26	0.008
F	2		2	low	414.0	0.00267	1.05E-03	4.19	1.76E-04	162	15.2	27	0.009
G					414.0	0.00108	6.35E-04	2.54	6.23E-05	243	17.3	24	0.004
H					421.2	0.00108	1.13E-03	4.52	6.58E-05	441	16.4	26	0.005
I	3		3	ultra-low	327.6	0.00014	1.35E-04	2.70	3.60E-05	316	3.9	84	0.116
J					446.4	0.00014	2.20E-04	4.40	6.37E-05	701	2.2	203	0.027
K					424.8	0.00007	1.28E-04	2.56	2.82E-05	777	2.5	171	0.011
L	4		4	highest	432.0	0.00786	2.89E-03	4.51	1.98E-04	159	39.6	11	0.028
M					414.0	0.00800	2.02E-03	3.15	2.31E-04	104	34.7	12	0.033
N	5	EW	5	moderate	432.4	0.00150	2.88E-03	1.50	6.62E-05	830	22.7	19	0.005
O					429.1	0.00300	5.76E-03	3.00	1.23E-04	824	24.3	18	0.012
P					428.0	0.00500	7.68E-03	4.00	1.66E-04	657	30.1	14	0.009
Q					427.0	0.00500	9.60E-03	3.00	2.05E-04	820	24.4	18	0.008

Table 10: Summary of Pilot-scale Refining Trials results

Several observations can be made from Table 10. The value of *H* for the Escher-Wyss refiner is similar to that for the Double Disc refiners when comparisons are made at a similar consistency, rotational speed and *SEL*. This is unexpected for the very coarse bar patterns of the EW. However, in this refiner, pulp circulates through it many times whereas pulp passes only once through the Double Disc refiners. Thus, extended

residence time can compensate for coarse bar pattern. Another unexpected result is the large values of *H* for the "ultra-low intensity" (Trials I – K) over an *SEL* range from 0.07 to 0.14 J/m. The low intensity in these trials was compensated for by a large number of impacts to give the same *SRE*, more than four times the number in other cases studied, to give the same refining energy. This suggests that number of impacts is a much stronger factor than intensity in determining homogeneity of treatment.

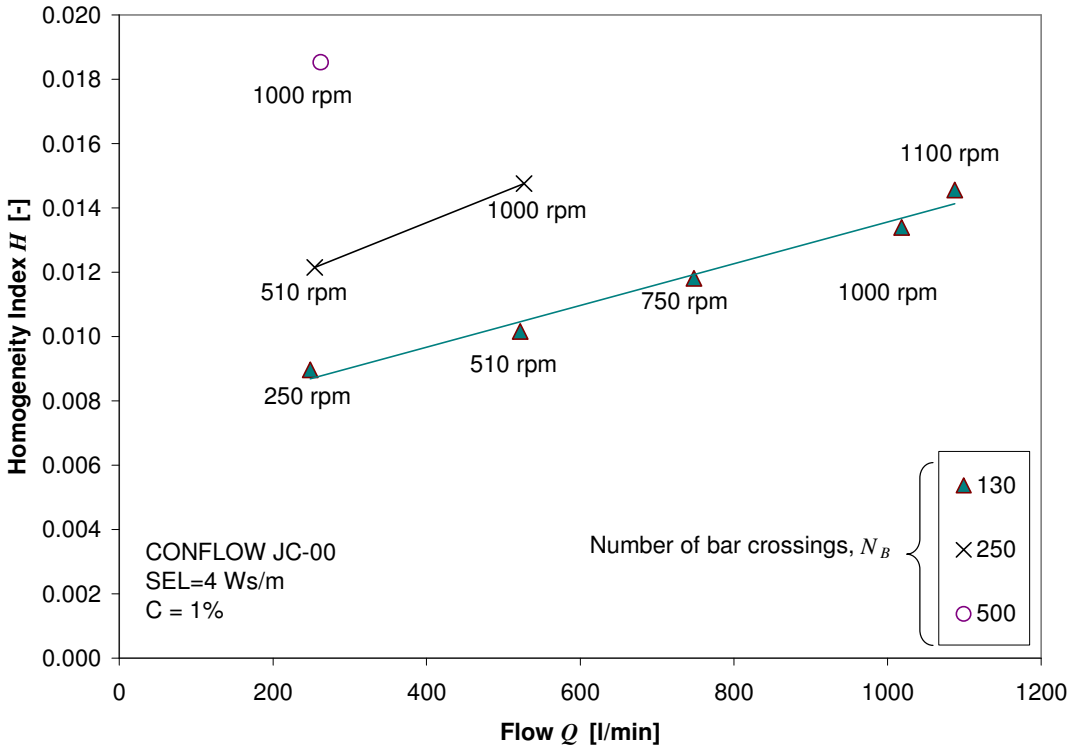

Figure 23: Homogeneity development in dependency of throughput and refiner speed using a CONFLO refiner at 1% consistency and *SEL* = 4 J/m

Flow conditions in refiners also affect *H*. This factor was evaluated in the CONFLO refiner by varying the rotational speed and throughputs while keeping the *SEL* constant. The findings are shown in Figure 23. It shows that for a given number of bar crossings, higher throughput flow rate increases refining homogeneity. This agrees with Figure 17 which showed that increasing radial velocity through a refiner increased the probability

of fibre impact at a bar crossing. The higher *H* may be due to more effective fibre mixing due to larger shear and turbulence.

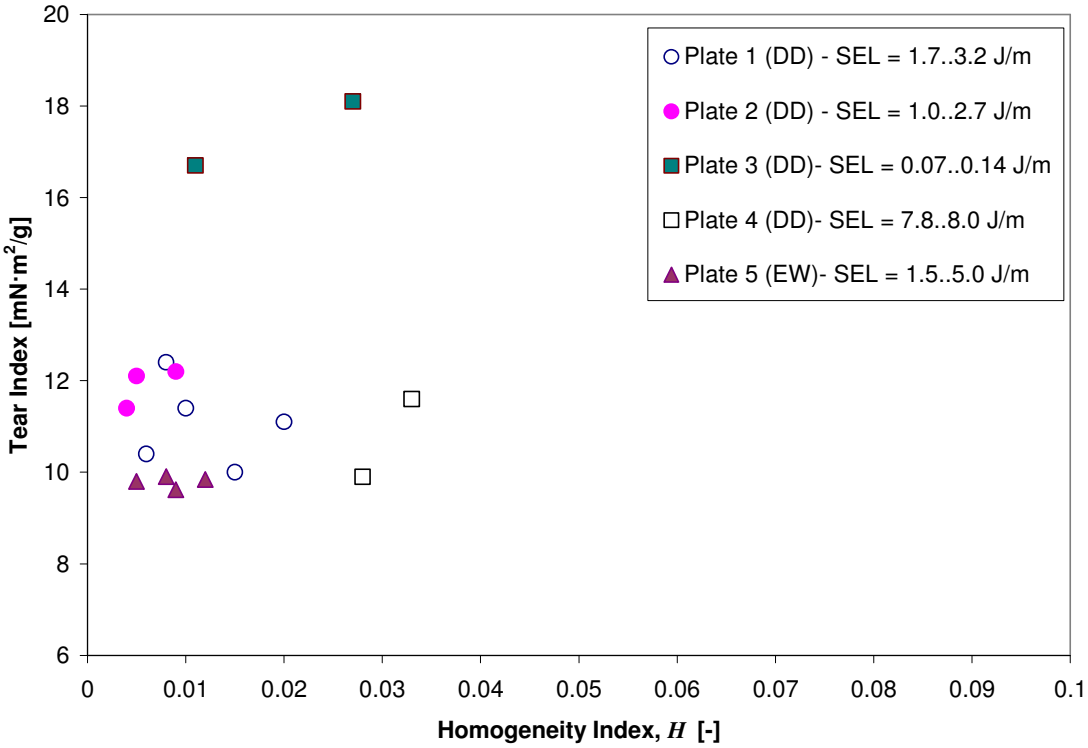

Figure 24: Relationship between Tear Index and Homogeneity Index, *H*.

Relationship between tear index and homogeneity is shown Figure 24. The ultra-low intensity plate (3) had the smallest loss in tear (shown as the largest tear strength). The other plates all caused a significant reduction in tear strength to the 10 – 12 mN·m^2/g range, with the largest intensity (*SEL*) accomplishing this with the greatest homogeneity. In summary, the experimental results described above show that the analysis depicted in Section 4 presents a useful basis for characterizing uniformity of treatment of pulp fibres in refiner. Moreover, the results show that previous estimates of intensities of impact are either too large or too small, and that the probability of impact corresponds with previous measurements of probability of successful loading cycle in compression refining.

7 Summary and Conclusions

A method to measure heterogeneity of treatment in pulp refiners has been developed using comminution theory and measurements of fibre length before and after refining. This was accomplished by interpreting the selection and breakage functions of the comminution equation in terms of a single bar crossing event, namely probability of impact with fibres, intensity distribution of impact, and location of breakage along a fibre length. These probabilities were interpreted in terms of heterogeneity of treatment.

The method was applied to measure heterogeneity of treatment in three different types of refiners: a pilot disc refiner, an industrial disc refiner, and an Escher-Wyss laboratory refiner. This was accomplished by regression fitting the comminution equation to measured fibre length distributions before and after refining under various operating conditions. The measured probabilities and intensities of impact showed some key findings:

- probability of fibre impact at a bar crossing event increases with decreasing groove depth and increasing groove width up to about a groove width of 10 mm, then decreases
- probability of fibre impact at a bar crossing event increases with radial pulp flow velocity
- intensity levels were larger than those predicted by Leider and Nissan/1977[36] and smaller than those predicted by Kerekes/1990[55]
- increase in tensile strength of pulp with refining was consistent with the cumulative probability of experiencing a loading cycle during a bar crossing

event, in agreement with the findings of Goosen et al./2007[86] for loading cycles in compression refining

The results of this work enable refining heterogeneity to be characterized in a number of different ways. A simple one, chosen somewhat arbitrarily, is a "Homogeneity Index", defined as the number of impacts on fibres having the average fibre length multiplied by the fraction of intensities within +/- 2 kJ/kg of the average intensity, divided by the specific refining energy. This index provided quantitative measurement of factors affecting homogeneity, postulated qualitatively by earlier workers, such as:

- increased flow rate through the refiner increased homogeneity of treatment
- large numbers of impacts at low intensities give greater homogeneity at a given specific energy than do smaller numbers of impacts at higher intensities
- large residence time in refiners can offset heterogeneity caused by very coarse bar pattern

8 Recommendations

This thesis has established a foundation upon which future work can build. This work could take several forms, for example further development of the method or applying it to refiners to correlate results with changes in pulp properties.

For further development of the approach, perhaps the greatest need is a measurement of the amount of pulp captured in a refiner gap, the variable called m_T in this thesis. Predicted values of intensity from this work seem reasonable, falling between values predicted by other workers. However, a definitive measurement linked to refiner variables which affect m_T would be of great value.

Another further development could be the use of force rather than energy as the basis of intensity related to strain and rupture of fibres. To obtain such forces, detailed knowledge of fibre distribution in refiner gaps, as well as the amount of fibres is needed.

On the question of applying this method, a comprehensive set of experiments ought to be carried out in which key pulp properties are linked to homogeneity of treatment defined in several ways.

In applying the method to mill refiners, it is recognized that most refiners are operated to minimize fibre cutting. Consequently the concept of a “bump test” should be explored in which power is increased for a short period to deliberately cut fibres for this test. While the conditions of a bump test differ from the operating condition, the difference can be

taken into account in the analysis to obtain a useful characterization of homogeneity of treatment obtained.

Lastly, there are other potential "homogeneity indices" than the one presented here. These should be explored. Perhaps the benefits of a two-parameter index outweigh the simplicity of a one-parameter index, and this too should be explored.

References

[1] Higgins, H. G., and J.de Yong. The beating process: Primary effects and their influence on pulp and paper properties. In The formation and structure of paper: Transactions of the symposium held at Oxford, September 1961, ed. F. Bolam. London: Technical Section, British Paper and Board Makers' Association. 2, 651–97 (1962).

[2] Page, D.H., The mechanism of strength development of dried pulps by beating. Svensk Papperstidning 88(3), R30-R35 (1985).

[3] Seth, R.S., Optimizing reinforcement pulps by fracture toughness. TAPPI Journal 79(1), 170-178 (1996).

[4] Hiltunen, E., Kettunen, H., Laine, J. E., Paulapuro, H., Behaviour of reinforcement fibres in TMP-based paper. Paperi ja Puu – Paper and Timber, vol. 84, no 4, pp. 269-273 (2002)

[5] Atack, D., Towards a theory of refiner mechanical pulping. Appita Journal 34(3): 223-227 (1980).

[6] Page, D., The Beating of Chemical Pulps--The Action and Effects. Trans. of Fundamental Symposium (F. Bolam Ed.) Tech. Sect. BP&BMA Oxford (1989).

[7] Danforth, D.W., The effect of refining parameter on paper properties. Advances in refining technology, PIRA, England (1986).

[8] Page, D.H., Ksky, J., Booth, D., Some initial observations on the action of the beater: What are we doing? BP + BMA Bull. 28, 1 – 7 (1962).

[9] Atack, D., Advances in beating and refining. Trans. Fund. Res. Symp., Oxford, Pulp and Paper Fundamental Research Society, UK, pp.261– 269 (1977).

[10] Ebeling, K., A Critical Review of Current Theories for the Refining of Chemical Pulps. International Symp. On Fund. Concepts of Refining, IPST, Appleton USA, pages 1-33 (1980).

[11] Hietanen S. – Development of a fundamentally new refining method. Paperi ja Puu. 72(9):874 (1990).

[12] Hietanen S., Ebeling K., A new hypothesis for the mechanics of refining. Paperi ja Puu 72(2):37-44 (1990).

[13] Mohlin U-B., Miller J., Industrial refining - effects of refining conditions on fibre properties. 3rd International refining Conference and Exhibition, March 20-22, Atlanta, USA. PIRA, paper 4 (1995).

[14] Seth R.S., The importance of fibre straightness for pulp strength. Pulp & Paper Canada 107(1): T1-T9 (2006).

[15] Mohlin, U.-B., Cellulose fibre bonding. Part 3. The effect of beating and drying on interfibre bonding. Svensk Papperstidning. 78(9), 338-341 (1975).

[16] Kerekes, R.J., Tam Doo, P.A., Wet fibre flexibility of some major softwood species pulped by various processes. 71st Annual Meeting, CPPA. Montreal, Canada, January 29-30, Preprints A, 45-46 (1985).

[17] Paavilainen, L., Conformability - flexibility and collapsibility - of softwood sulphate pulp fibres. Paperi ja Puu 75(9-10), 689-702 (1993).

[18] Page, D.H., De Grace, J.H., Delamination of fiber walls by beating and refining. TAPPI Journal, Vol. 50(10), 489-495 (1967).

[19] Clark J.D., Fibrillation, free water, and fiber bonding. TAPPI Journal, Vol. 52(2):335-340 (1969).

[20] Hartman, R.R., Mechanical treatment of pulp fibers for paper property development. Transactions of the Eighth Fundamental Research Symposium held at Oxford, England, September 1985. Mechanical Engineering Publications Limited, London, Vol. 1, 413-442 (1985).

[21] Kerekes, R.J. Perspectives on Fiber Flocculation in Papermaking. Proceedings International Paper Physics Conference, Niagara-on-the-lake, ON, Canada, pp.23-31 (1995).

[22] Mohlin, U-B., Low consistency beating - laboratory evaluation contra industrial experience. Current and future technologies of refining, Conference Proceedings. 10-12 December 1991. PIRA, Leatherhead, UK. Volume 1, Paper 01, 14 pages (1991).

[23] Seth, R.S., Zero-span tensile strength of papermaking fibres. Paperi ja Puu 83(8), 597-604 (2001).

[24] Smith, S.F., The action of the beater in papermaking. Paper Trade Journal 106(26):47 (1922).

[25] Rance, H. F., In Symposium on Beating. Proceedings Technical Section British Paper and Board Makers' Association 32(2):360-70 (1951).

[26] Steenberg, B., In Symposium on Beating. Proceedings Technical Section British Paper, and Board Makers' Association 32(2):388-95 (1951).

[27] Frazier, W.C., Applying hydrodynamic lubrication theory to predict refiner behavior. Journal of Pulp and Paper Science, Vol.14 No. 1, J1-J5 (1988).

[28] Roux, J.C, Hydrodynamic modelling of the behaviour of the pulp suspensions during beating and its application to optimising the refining process. 11th Fundamental Research Symposium, Cambridge, UK, 21-26 September (1997).

[29] Lundin, T., Lönnberg, B., Harju, K., Soini, P., LC - Beating of Pulp Fibres. Pulping Conference Proceedings, (1999).

[30] Halme, M., Syrjanen, A., Flow of stock in a conical refiner as observed by high speed film camera, Atti. Cong. Eur. Tech. Carteuria, Venice, PIRA, pp. 273– 277 (1964).

[31] Herbert, W. and Marsh, P.G., Mechanics and Fluid Dynamics of a Disk Refiner. TAPPI Journal, Vol. 51, No. 5, pp. 235-239 (1968).

[32] Banks, W.A., Design considerations and engineering characteristics of disc refiners. Paper Technology 8 (4), 363– 369 (1967).

[33] Goncharov, V.N., Force factors in a disc refiner and their effect on the beating process. Bum. Prom. 5, 12–14 (1971).

[34] Fox, T.S., Brodkey, R.S., Nissan, A.H., High speed photography of stock transport in a disc refiner. TAPPI Journal, Vol. 62 (3), 55– 58 (1979).

[35] Leider, P.J., Rihs, J., Understanding the disk refiner, TAPPI Journal, Vol.60, no.9, pp.98-102 (1977).

[36] Leider, P.J., Nissan, A.H., Understanding the disc refiner—the mechanical treatment of fibres, TAPPI Journal, Vol. 60 (10), 85– 89 (1977).

[37] Fox, T. S., Pulp transport in the disk refiner. Paper presented at the 50th anniversary of The Institute of Paper Chemistry, Appleton, WI, p.49 (1979).

[38] Arjas, A., Jankola, 0., and Ryti, N., Paperi ja Puu 51(12):869-79 (1969).

[39] Batchelor, W.J. and Lundin, T., - A method to estimate fibre trapping in low consistency refining. TAPPI Journal, Vol. 5(8):31 (2006).

[40] Kerekes R.J., Olson J.A.: Perspectives on fibre length. reduction in refining. In: proceedings of 7th PIRA. international refining conference & exhibition, In: proceedings of 7th PIRA international refining conference &. exhibition, 25-26 March, Stockholm, Sweden, March 25-26, paper 5 (2003).

[41] Steenberg, B. – Mahlungsvorgaenge – Neue Betrachtungen – Das Papier, Darmstadt, 35, 10A S. V141-V149 (1979).

[42] Goosen, D., Olson, J.A., Kerekes, R.J., The Role of Heterogeneity in Compression Refining. Journal of Pulp and Paper Science, 33(2):110-114 (2007).

[43] Goncharov, V.N., Force Factors in a Disk Refiner and Their Effect on the Beating Process. Bum. Promst. 12(5): 1-14 (1971).

[44] Martinez, D.M., Batchelor, W.J., Kerekes, R.J., and Ouellet, D., - Forces on fibres in refining - normal force. Journal of Pulp and Paper Science, 23(1):J 11 (1997).

[45] Batchelor, W.J., Martinez, D.M., Kerekes, R.J., and Ouellet, D., - Forces on fibres in refining - shear force. Journal of Pulp and Paper Science, 23(1):J 40 (1997).

[46] Kerekes, R.J., Senger, J.J., Characterizing Refining Action in Low-Consistency Refiners by Forces on Fibres. Journal of Pulp and Paper Science 32(1):1-8 (2006).

[47] Koskenhely, K., Nieminen, K., Paulapuro, H., Edge form profile of refiner filling bars and its impact on softwood fibre shortening. Paperi ja Puu, vol. 89, no4, pp. 236-241 (2007).

[48] Wultsch, F., Flucher, W., Der Escher-. Wyss-Kleinrefiner als Standard Prüfgerät für moderne Stoffaufbereitungsanlagen. Das Papier 12(13):334-342 (1958).

[49] Brecht, W., Siewert,W.H., Zur theoretisch-technischen. Beurteilung des Mahl-prozesses modern Mahlmaschinen. Das Papier 20(10):4-14 (1966).

[50] Lumiainen, J., "A new approach to the critical factors effecting on refining intensity and refining results in low consistency refining", TAPPI Papermakers Conference Proceedings, TAPPI Press, Atlanta (1990)

[51] Meltzer, F.P., Rautenbach, R., Neue Moeglichkeiten zur Vorherbestimmung des technologischen Mahlergebnisses. Das Papier 48 (9), 578– 583(1994).

[52] Lewis, J., and Danforth, D. W., Stock preparation analysis. TAPPI Journal 45(3):185-88 (1962).

[53] Danford, D.W., Southern Pulp and Paper Manufacturer, pp. 52 (1969).

[54] Van Stiphout, J. M. J., A preliminary study of refining action on cellulose fibers. TAPPI Journal, 47(2):189A-91A (1964).

[55] Kerekes, R.J.; Characterization of pulp refiners by a C-factor. Nordic Pulp and Paper Journal 5(1), p.2-8 (1990).

[56] Steenberg, B., Svensk Papperstidning 66(22):933-939 (1963).

[57] Halme, M., Paperi ja Puu 44(12):658-60 (1962).

[58] Ryti, N., and Arjas, A., Paperi ja Puu 51 (1): 69 (1969).

[59] Olson, J.A., Drozdiak, J., Martinez, M., Garner, R., Robertson, A., Kerekes, R.J., Characterizing fibre shortening in a low-consistency refining using a comminution model. Powder Technology 129, pp. 122–129 (2003).

[60] Batchelor, W.J. and Lundin, T., - A method to estimate fibre trapping in low consistency refining. TAPPI Journal, 5(8):31 (2006).

[61] Batchelor, W. and Ouellet, D., - Estimating forces on fibres in refining. Proceedings 4th International Refining Conference, PIRA International, Leatherhead, U.K., p Paper 2 (1997).

[62] Roux , J.C., Joris, G., Angular parameters beyond specific edge load. TAPPSA Journal, No. 7, (2005).

[63] Endres, I., Vomhoff, H., Ström, G. New Sensor Technique for Measuring Small-Scale Pressure Distributions. International Paper Physics Conference, Victoria, BC (2003).

[64] Prairie, B., Wild, P., Byrnes, P., Olender, D., Francis, D.W., and Ouellet, D., Forces During Bar-Passing Events in Low Consistency Refining: Effects of Refiner Tram. Pulp & Paper Canada, 109(9):T153-T156 (2007).

[65] Page, D.H., The origin of the differences between sulphite and kraft pulps. Journal of Pulp and Paper Science, March TR 15-TR20 (1983).

[66] Hietanen, S.; The Role of Fiber Flocculation in Chemical Pulp Refining. Paperi ja Puu - Paper and Timber 73(3): 249-259 (1991).

[67] Lumiainen, J. – Comparison of mode of operation of conical and disc refiners. PTS-IZP 1.CALAR-Symposium, 01.12.1995, Heidenau, GER (1995).

[68] Simons, F. L., TAPPI Journal 33(7):312-4 (1950).

[69] Nisser, H. & Brecht, W., 'Zwei neue Messkriterien von aufgeschwemmten Fasern zur Beurteilung der Blattfestigkeit', Svensk Papperstidning 66(2), pp. 37–41 (1963).

[70] Mohlin, U-B., and O. Lidbrandt, Changes in fiber structure due to refining as revealed by SEM. Pages 61-74 in International symposium on fundamental concepts of refining. Appleton, WI. (1980).

[71] Dharni, S., Kerekes, R.J.; Estimation of the number of impacts imparted to the pulp in a disc refiner. Master of Pulp and Paper Eng. Project Report, UBC Pulp and Paper Centre (1989).

[72] Dekker, J.C., How many fibres see the refiner? Amount of changed fibres measured by RBA. PIRA Refining and Mechanical Pulping. Conference, March 2-3, Barcelona, Spain (2005).

[73] Dillen, S, Heterogeneity – an important parameter in low consistency refining. Intl Symp of Fundamental Concepts of Refining IPC, The Institute of Paper Chemistry, Appleton, pp. 331 (1980).

[74] Epstein, B., Logarithmic-normal distribution in breakage of solids, Ind. Eng. Chem. 40 (12), 2289 (1948).

[75] Reid, K.J., "A Solution to the Batch Grinding Equation" Chemical Engineering Science Vol. 20, pp. 953-963 (1965).

[76] Austin, L.G., Introduction to the Mathematical Description of Grinding as a Rate Process. Powder Technology, 5, p. 1-17 (1971-1972).

[77] Kane, M.W., The fissioning of filaments by a uniform and continuing effect, TAPPI Journal 40 (9), 234A– 238A (1957).

[78] Meyer, R., Almin, K.E., Steenberg, B., Length reduction of fibres subject to breakage. British Journal of Applied Physics. 17, 409–416 (1966).

[79] Roux, J.C., Mayade, T.L., Modeling of the particle breakage kinetics in the wet mills for the paper industry. Powder Technology 105, 237– 242 (1999).

[80] Corte, H., Agg, S., On the shortening of pulp fibres during beating. International Symposium on Fundamental Concepts of Refining, Sept., pp. 149– 157, Institute of Paper Chemistry (IPC), (1980).

[81] Koka, V.R., Trass, O., Estimation of breakage parameters in grinding operations using a direct search method. Int. J. Miner. Process. 23, 137– 150 (1988).

[82] Corson, S.R., Probabilistic model of the disc refining process. Svensk Papperstidning 2 (31), 57– 64 (1972).

[83] Strand, B.C., Mokvist, A., The application of comminution theory to describe refiner performance. Journal of Pulp and Paper Science, 15 (3), J100– J105 (1989).

[84] Berthiaux, H., Analysis of Grinding Processes by Markov Chains. Chemical Engineering Science, 55, 4117-4127 (2000).

[85] Ellis, R.L. and Rudie, A.W., Ideal Fibres for Pulp and Paper Products. IPST Technical Paper Series, Number 384, (1991).

[86] Goosen, D. R. Olson, J. A. Kerekes, R. J., The Role of Heterogeneity in Compression Refining. Journal of pulp and paper science, VOL 33; Numb. 2, pages 110-114 (2007).

[87] Page, D. H., F. El-Hosseiny, K. Winkler, and R. Bain, The mechanical properties of single wood-pulp fibres. Part 1: A new approach. Pulp and Paper Magazine of Canada, 73(8):72-77 (1972).

[88] Mark. R. E., Borch, J., Habeger, C. C., Lyne, B. M., Handbook of Physical Testing of Paper: Volume 1, Second Edition, illustrated, revised, published by CRC Press, ISBN 0824704983, 9780824704988, page 56, (2001).

[89] Page, D. H., and El-Hosseiny, F., The mechanical properties of single wood pulp fibres. Pt 4: The influence of defects. Svensk Papperstidning 14:471-474 (1976).

[90] Berthiaux, H., Dodds, J., A New Estimation Technique for the Determination of Breakage and Selection Parameters in Batch Grinding. Powder Technology 94, 173-179 (1997).

[91] Bertrand, D., Guibert, D., Melcion, J.-P., Duc, G., Evaluation of the transition matrix for comminuting pea seeds in an impact mill using a linear neural network, Powder Technology 105, 119–124 (1999).

[92] Pettersen, J. K., Sandvik, L., Estimating the breakage and selection functions for a continuous mill. International journal of mineral processing, Vol. 35, No3-4, pp. 149-158 (1992).

[93] Fan, L. T., Too, J. R., & Nassar, R., Stochastic simulation of residence time distribution curves. Chemical Engineering Science, 40(9), 1743 (1985).

Appendices

Appendix A: Distributions of Intensity in Refiner Gaps

Once fibres are within the gap between refiner bars, there is a distribution of forces acting upon individual fibres. Clearly, this distribution is complex and can only be modeled approximately. We do so here by considering the pulp to be a mat upon which an average force is exerted that produces a distribution of local pressures. We consider the distribution to be similar to that acting on a wet pad of pulp.

In recent work, Endres et al./2005[63] measured pressure distributions on pulp pads and found distributions of the type shown in Figure A.1. This can be represented by a Gamma distribution function, i.e. by equation (A.1), which is essence may represent a range of possible distributions by differing values of α, a shape parameter and β, a scale parameter.

$$p_{Gamma}(I) = \frac{1}{\beta^{\alpha} \cdot \Gamma(\alpha)} \cdot I^{\alpha-1} \cdot e^{-\frac{I}{\beta}} \tag{A.1}$$

Given the very approximate nature of our estimated pressure distributions in the gap of refiners, we chose a simple form of the gamma distribution (α = 2, β = 11). This gamma function is shown in Figure A.1 superposed on Endres' measured pressures. For the purpose of this study, we consider local intensity, I, to have the same distribution as local pressure. Therefore we may express the probability distribution of I, p_I,(I) as

$$p_I(I) = aIe^{-bI} \tag{A.2}$$

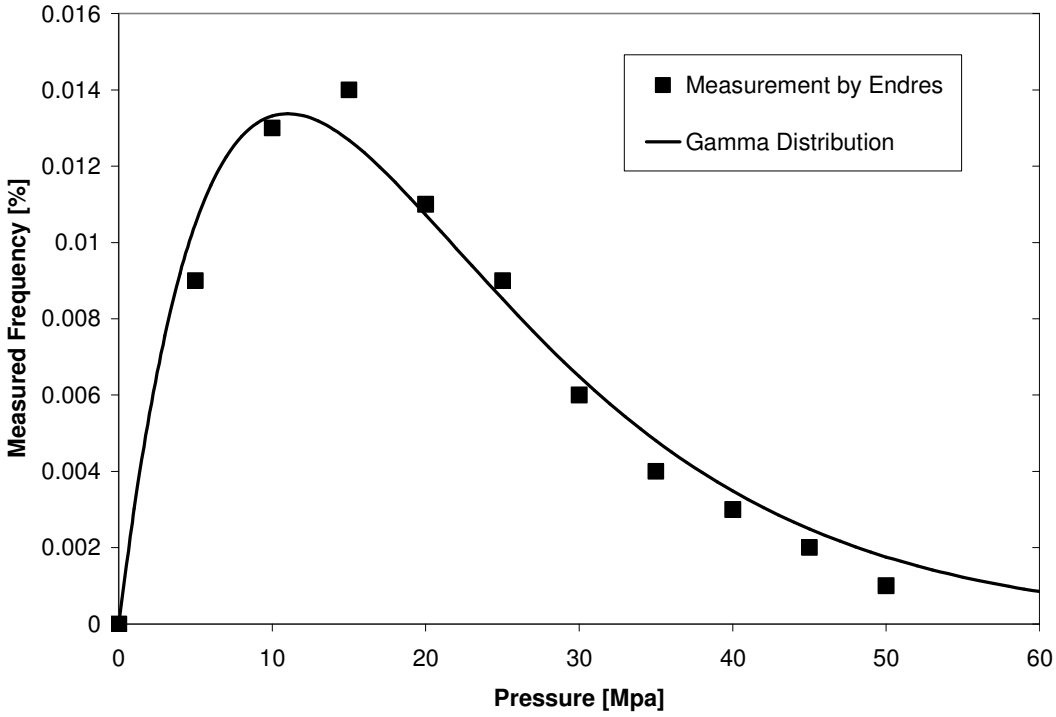

Figure A.1: Pressure Distribution within a fibre flock covering a 8 x 8 mm area, at ≈ 30% consistency measured by Endres et al./2005[63]

Prairie et al./2007[64] have shown that in a refiner gap, under low consistency conditions, compression forces are large, about 10 times the shear forces, and therefore are likely to vary in a similar manner to the measurements of Endres.

Appendix B: Integration of Pressure Distribution

Here we determine the parameters in the pressure distribution on pulp mat cited in Appendix A.

$$p_I(I) = aIe^{-bI} \tag{B.1}$$

First, we determine the relationship between a and b by normalizing the distribution

$$\int_0^\infty p_I(I)dI = 1\,[\mathrm{kJ}/kg] \tag{B.2}$$

$$\int_0^\infty aIe^{-bI}\,dI = \frac{a\left(-bxe^{(-bx)} - e^{(-bx)}\right)}{b^2}\Bigg|_0^\infty = 1\,[\mathrm{kJ}/kg] \tag{B.3}$$

$$\frac{a}{b^2} = 1[kJ/kg] \tag{B.4}$$

$$\therefore b = \sqrt{\frac{a}{1[kJ/kg]}} \tag{B.5}$$

Next we determine values of a and b in terms of average intensity I_A.

$$\int_0^\infty p_I(I)IdI = 1[kJ/kg]\cdot I_A \tag{B.6}$$

Upon substitution of equation (B.5) into (B.1) we obtain

$$\int_0^\infty I^2 \cdot a \cdot e^{-\sqrt{\frac{a}{1[kJ/kg]}}I}\,dI = 1[kJ/kg]\cdot I_A \tag{B.7}$$

$$\frac{2\cdot 1[kJ/kg]}{\sqrt{\frac{a}{1[kJ/kg]}}} = 1[kJ/kg]\cdot I_A \tag{B.8}$$

$$\frac{2}{I_A} = \sqrt{\frac{a}{1[kJ/kg]}} \tag{B.9}$$

$$\therefore a = \frac{4 \cdot 1[kJ/kg]}{I_A{}^2} \tag{B.10}$$

Substituting equation (B.10) into (B.5) gives:

$$b = \sqrt{\frac{4 \cdot 1[kJ/kg]}{I_A{}^2 \cdot 1[kJ/kg]}} = \frac{2}{I_A} \tag{B.11}$$

This gives

$$p_I(I) = \frac{4 \cdot 1[kJ/kg]}{I_A{}^2} \cdot I \cdot e^{-\frac{2}{I_A} \cdot I} \qquad \text{with } I_A = \frac{SEL}{m_T} \tag{B.4}$$

For simplicity, the dimension *[kJ/kg]* of the normalization to *1* is not be shown in subsequent equations.

Appendix C: Fibre Strength Distributions

Fibres in a sample of pulp to not have equal strength. Many factors contribute to the distribution of strength among fibres, one of which is the fibril angle. The dependence of tensile strength of individual fibres on fibril angle found by Page et al./1972[87] is shown in Figure C.1.

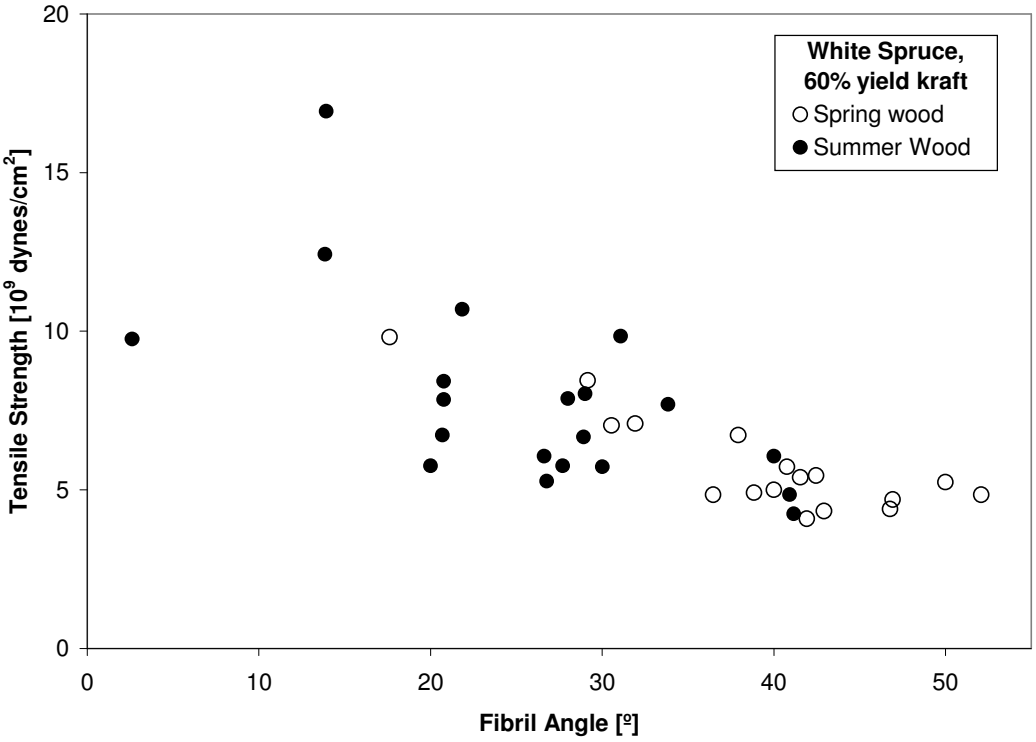

Figure C.1: Tensile strength vs. fibril angle for springwood and summer wood fibre of white spruce, reproduced from Page et al./1972[87]

In this study, we estimate fibre strength by the energy needed to rupture a fibre in tension, calling this the average rupture intensity I_C. We then consider distributions of rupture intensity.

C.1 Average Rupture Intensity I_C

From Hooke's law it is known that:

$$\sigma = \frac{F_{\max}}{A_F} \tag{C.1}$$

with σ stress (tensile strength), *[N/m²] = [Pa] = [dyne/cm²]*

F_{max} maximum force, *[N]*

A_F cross sectional area, *[m²]*

$$EM = \frac{\sigma}{\varepsilon} \tag{C.2}$$

with EM elastic modulus (Young's modulus), *[Pa]*

σ stress (tensile strength), *[N/m²]*

ε elastic strain (dimensionless)

Specific energy, I_C, required to strain a single fibre is given by:

$$I_C = \frac{1}{\rho} \cdot \frac{1}{2} \cdot EM \cdot \varepsilon^2 \qquad \left[\frac{N/m^2}{kg/m^3}\right] = \left[\frac{N \cdot m}{kg}\right] = \left[\frac{J}{kg}\right] \tag{C.3}$$

with ρ is cell wall density, *[kg/m³]*

If straining occurs under shock conditions, a state of unaxial strain results, and the above energy is increased (Mark et. al/2001[88]), as shown below:

$$I_C = \frac{1}{\rho} \cdot \frac{1}{2} \cdot EM \cdot \varepsilon^2 \cdot \frac{(1-\upsilon)}{(1-2\cdot\upsilon)\cdot(1+\upsilon)} \tag{C.4}$$

with υ Poisson ratio

We estimate a strain of 10% as the level necessary to deform a fibre in tension to the point of fibre rupture. Other parameters are:

$\upsilon = 0.35$

$\rho = 1500\ [kg/m^3]$

Thus, the specific energy for rupture can be expressed as:

$$I_C = \frac{1}{1500\left[kg/m^3\right]} \cdot \frac{1}{2} \cdot EM \cdot (0.1047)^2 \cdot \frac{(1-0.35)}{(1-2\cdot 0.35)\cdot(1+0.35)} \tag{C.5}$$

From Page et al./1976[89] data we can calculate an average Young's modulus for the white spruce fibres as:

$$EM_{average} = \frac{\sigma_{average}}{\varepsilon} = \frac{0.659 \cdot 10^9\left[Pa\right]}{0.1047} = 6.57GPa \tag{C.6}$$

$$I_{C,average} = 5.864 \cdot 10^{-6}\left[m^3/kg\right] \cdot 6.57\left[GPa\right] \tag{C.7}$$

$$\therefore I_{C,average} = 38.55\left[kJ/kg\right] \tag{C.8}$$

This rupture intensity value may vary from furnish to furnish. For simplicity we estimate the average rupture strength of white spruce fibres is around 35 kJ/kg.

C.2 Distribution of Rupture Intensity

Fibres have a range of fibre strength I_C. Little has been published on this. The available information (D.H. Page and F. El-Hosseiny/1976[89]) is shown in Figure C.2:

Figure C.2 has been removed due to copyright restrictions. The information removed is decribed in the Figure description below. The reference source is: Page, D. H., and El-Hosseiny, F., The mechanical properties of single wood pulp fibres. Pt 4: The influence of defects. Svenk. Papperstidn. 14:471-474 (1976)

Figure C.2: Frequency distribution of tensile strength for black spruce acid sulphite fibres, pulped to 63% yield, at 0.42 and 1.50 span length, reproduced from Page et al./1976[89]

We replaced the distribution in Figure C.2 by a Weibull distribution function shown below in terms of a probability of rupture at an intensity equal to the average rapture strength, $p_C(I_C)$.

$$p_C(I_C) = \frac{k}{\lambda^k} \cdot {I_C}^{k-1} \cdot e^{-\left(\frac{I_C}{\lambda}\right)^k} \qquad \text{(C.9)}$$

with k shape parameter

λ scale parameter

Considering the lack of knowledge concerning the functional form of rupture distribution functions, the data may be approximated by a Gamma functions as well, as shown in Figure C.3.

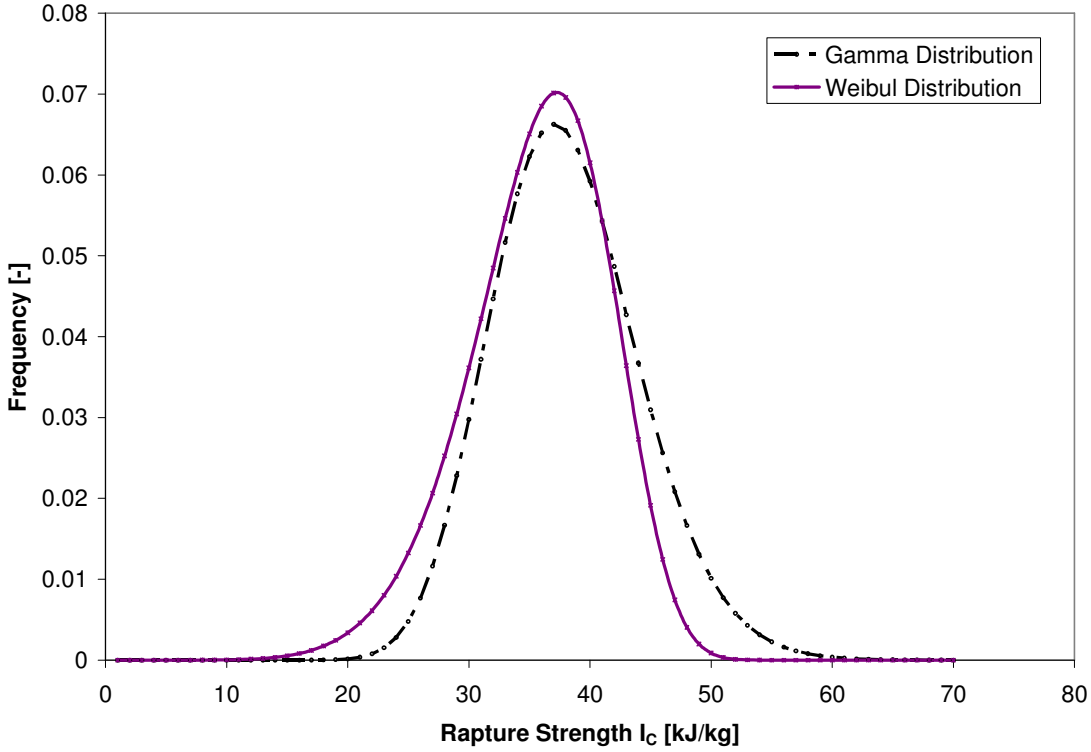

Figure C.3: Comparison of the calculated rupture strength distribution of White Spruce fibres using Gamma and Weibull probability distribution functions

We may estimate the parameter of $p_C(I_C)$ for the Weibull distribution function based on the assumed $I_{C,average} = 35\ [kJ/kg]$ and a standard deviation of $5.9\ [kJ/kg]$ to be $k = 7$ and $\lambda = 37.41\ [kJ/kg]$.

Therefore, equation (C.9) becomes:

$$p_C(I_C) = 1[kJ/kg] \cdot \frac{7}{37.41^7 [kJ/kg]^7} \cdot {I_C}^6 \cdot e^{-\left(\frac{I_C}{37.41[kJ/kg]}\right)^7} \qquad \text{(C.10)}$$

Appendix D: Breakage and Selection Functions

During comminution, the number of fibres of length *i* decreases due to shortening of fibres of size *i* to smaller sizes, and increases its numbers to the shortening of larger sizes *j* to size *i*. The Breakage Function B_{ij} reflects the probability of fibres of length *j* being shortened to size *i* as shown by Berthiaux/2000[84]. These changes are described in terms of incremental energy input by the comminution equation (equation (9) in text), which can be rewritten as the following matrix form:

$$\frac{dn}{dE} = A \cdot n \tag{D.1}$$

$$\text{where } A = \left(B - I_n\right) \cdot S \tag{D.2}$$

Here, *n(E)* is a column vector whose entries are the n_i fibre length fraction in each size interval after the energy input, *E*. When referring to size intervals indexed from 1 (for the longest fibres) to *m* (for the shortest fibres and fines), Breakage and Selection functions can be represented by matrix notation, denoted by *B* the breakage matrix (whose elements are B_{ij}) and by *S* the selection matrix (whose elements are S_i). It is assumed here, that fibres can only undergo length reduction during refining; *B* is a lower triangular matrix. *S* is a diagonal matrix. Upon multiplication with the identity matrix, I_n, *A* becomes a lower triangular matrix. The solution of equation (D.1) can be made by diagonalization of *A*, introducing matrix U_T as the matrix of the eigenvectors. Thus, it can be demonstrated that

$$n(E) = V(E) \cdot n(0) \tag{D.3}$$

$$V(E) = U_T \cdot R_D(E) \cdot U_T^{-1} \tag{D.4}$$

$$A = -U_T \cdot S \cdot U_T^{-1} \tag{D.5}$$

V(E), the so called transition matrix, is a lower triangular matrix which depends on the energy of refining through the previous set of equations, in which $R_D(E)$ is a diagonal

matrix whose entries are $e^{(-S_i \cdot E)}$. A process is said Markovian if *V(E)* is only dependent on the current state and not on the previous states. One can assume that *V(E)* remains constant for a serious of batch refining processes – which can be linked to a continuous refining. In this case, the evolution of the system is given by:

$$n_{t+1} = V(E) \cdot n_t \tag{D.6}$$

If *V(E)* is known, n_t may be determined from an initial state vector n_0:

$$n_t = V(E)^t \cdot n_0 \tag{D.7}$$

where $V(E)^t$ is the matrix *V(E)* raised to power *t*.

The estimation of *V(E)* is not straightforward and is difficult to be achieved by a usual linear regression. The assessment of *V(E)* from experimental data is still a subject of study. In this case, the simple matrix calculation may be very difficult or unstable. In recent work, Berthiaux and Dodds/1997[90] have illustrated the difficulties in such assessments and have presented a new estimation technique of breakage and selection parameters in batch grinding. This method has been tested (see Appendix E). Their method requires a prior smoothing of the fibre length distribution. To assess the transition matrix for a given refining step, we employ the approach of Bertrand et al./1999[91]. The transition matrix *V(E)* has some constraints, which are listed below:

1*. As the elements of *V(E)* are probability values, they are null or positive and less than 1: $0 \le v_{ij} \le 1$.

2*. If we suppose that there are no losses during refining, the sum of each column of V must be equal to 1:

$$\forall j, \sum_{i=1}^{x} \mathrm{v}_{ij} = 1. \tag{D.8}$$

3* The size of a fibre cannot increase during refining. For $j>i$, we have $v_{ij}=0$.

In our work, we estimate the transition matrix $V(E)$ from experimental obtained sequence of fibre length histograms or distributions respectively, n_0, n_1, …, n_q (see Chapter 5). Following Bertrand et.al/1999[91], we employ a simple version of a monolayer neural network for the transition matrix estimation. This method does not require complex matrix manipulation or numerical assessment of derivatives. Using a sequence of fibre size histograms n_0 and n_{t+1} it is possible to estimate the transition probabilities v_{ij}.. The histograms can be obtained from experiments carried out in laboratory and industrial refiner (n_0, n_1, …,n_q). The basis of the approach is to step-by-step slightly modify the values of the transition probabilities in order to reduce the error of the model. When presenting a given vector n_t as input of the system, the least square error is given by:

$$error = \sqrt{\sum_{i=1}^{m} \left(n_{i,t+1} - out_i\right)^2} \tag{D.9}$$

where $n_{i,t+1}$ represents an element of the vector of expected (observed) value and out_i the estimated values assessed according to

$$out_j = \sum_{i=1}^{j} v_{ij} \cdot n_{i,t} \tag{D.10}$$

The method of *steepest descent* can be used for stepwise reducing the error. For this purpose, one must assess $(\partial \text{error})/(\partial \mathrm{v}_{ij})$, the change of error as a function of the change in the transition probability v_{ij}. It can readily be shown that $(\partial \text{error})/(\partial \mathrm{v}_{ij})$ is given by:

$$\frac{\partial error}{\partial v_{ij}} = n_{i,t}\left(out_j - n_{j,t+1}\right) \tag{D.11}$$

Decreasing the error value means a transition probability change proportional to $(\partial error)/(\partial v_{ij})$. The resulting algorithm is very simple and is given below.

(1) The weights (probabilities of the transition matrix) are initialized by giving them small positive random values, respecting the constraints (2^*).

(2) A discrete t value is randomly selected in the range from 0 to q -1.

(3) The observed histogram n_t is presented as input of the neural network.

(4) The elements of the output vector out_i is then assessed according to equation (D.10). The expected values are the elements of n_{t+1}.

(5) The weight (transition probabilities) is then modified according to:

$$v_{ij} \leftarrow v_{ij} + \mu \cdot n_{i,t}\left(n_{j,t+1} - out_j\right) \tag{D.12}$$

where μ, the learning rate parameter, is a positive value, less than 1.

(6) If a given weight v_{ij} is less than 0, it is replaced by 0.

(7) In order to respect constraint (2^*), the sum_j is then assessed, according to:

$$sum_j = \sum_{i=1}^{m} v_{ij} \tag{D.13}$$

The weights v_{ij} are then replaced by $(v_{ij})/(sum_j)$.

(8) After each number of iterations, the least-square error of the model is assessed from:

$$error = \sqrt{\frac{1}{m \cdot q}\sum_{t=1}^{q}\sum_{i=1}^{m}\left(n_{i,t} - out_{i,t}\right)^2} \tag{D.14}$$

If the error is larger than a given threshold, the procedure is iterated by performing again the steps (2) to (8). Otherwise, the procedure is finished. The steps (6) and (7) above are

specific of the current problem, and are needed in order to respect constraints (1^*) and (2^*), respectively.

Once the weight elements v_{ij} are obtained, the resultant transition matrix *V(E)* is then decomposed into its characteristic eigenvalue and eigenmatrix vectors and within it determine the selection function matrix *S*. It is then possible to use this information and equations (D.4) and (D.5) in order to determine the breakage probability matrix *B* by going back to equation (D.2).

Appendix E: Validation of Transition Matrix Approach

To validate our transition matrix method and Matlab™ calculation routines, we conducted a series of computation for which Transition matrix, or the selection function was known and compared them with our determined selection and breakage functions.

E.1 Assessment of the Transition Matrix

From a time sequence of particle size histograms Bertrand et.al/1999[91] assessed, using a linear neuron network, the transition matrix as described in Appendix D. Their estimated transition matrix is shown in Table E.1.

	>2500	2000	1600	1250	1000	800	630	500	400	315	250	200	<200
>2500	0.3882												
2000	0.1297	0.0493											
1600	0.1315	0.2008	0.2339										
1250	0.1068	0.2140	0.2581	0.3122									
1000	0.0635	0.1331	0.1687	0.2450	0.3336								
800	0.0461	0.0880	0.0969	0.1557	0.2587	0.3965							
630	0.0355	0.0670	0.0606	0.0869	0.1538	0.2680	0.4770						
500	0.0261	0.0584	0.0462	0.0502	0.0754	0.1351	0.2458	0.5551					
400	0.0195	0.0438	0.0298	0.0294	0.0375	0.0566	0.0975	0.2003	0.6315				
315	0.0136	0.0289	0.0230	0.0284	0.0355	0.0394	0.0526	0.0837	0.1493	0.7521			
250	0.0091	0.0214	0.0183	0.0221	0.0254	0.0253	0.0295	0.0388	0.0609	0.0622	0.8722		
200	0.0093	0.0348	0.0119	0.0039	0.0015	0.0006	0.0061	0.0031	0.0001	0.0538	0.0573	1.0000	
<200	0.0212	0.0604	0.0524	0.0662	0.0786	0.0786	0.0916	0.1190	0.1582	0.1319	0.0705	0.0000	1.0000

Table E.1: Transition matrix assessed by Bertrand et.al/1999[91]

As previously mentioned, the upper triangle of the matrix includes elements the probability of which is equal to 0. As there were 13 particle size classes, the matrix was dimensioned 13 x 13. The elements $V_{13,13}$ (bottom-right) on the table corresponded to the finest particle size. When the particles reached this state, they remained in this class and therefore the corresponding probability was equal to 1.

From this estimated transition matrix, we obtained an estimation of the particle size distributions. For this purpose, we applied equation (D.6) with $V(E)$ being the estimated transition matrix given in Table E.1, and n_t, the particle size distribution for a given

energy or passage. The initial particle size distribution was represented by a vector n_0 the elements of which are equal to 0, except the first one which is equal to 1. The resultant particle size distributions are shown in Table E.2.

	n_0	n_1	n_2	n_3	n_4	n_5
>2500	1	0.3882	0.1507	0.0585	0.0227	0.0088
2000	0	0.1297	0.0567	0.0223	0.0087	0.0034
1600	0	0.1315	0.1079	0.0564	0.0254	0.0107
1250	0	0.1068	0.1365	0.0987	0.0564	0.0284
1000	0	0.0635	0.1115	0.1059	0.0757	0.046
800	0	0.0461	0.0934	0.1095	0.0963	0.0708
630	0	0.0355	0.0788	0.1073	0.1124	0.0989
500	0	0.0261	0.0634	0.0946	0.1121	0.1137
400	0	0.0195	0.0463	0.0717	0.0916	0.1028
315	0	0.0136	0.0363	0.0614	0.0841	0.1014
250	0	0.0091	0.0259	0.0452	0.0641	0.0809
200	0	0.0093	0.0211	0.0306	0.0401	0.0505
<200	0	0.0212	0.0717	0.1378	0.2106	0.2839

Table E.2: Calculated evolution of particle size distribution

The estimated transition matrix using our proposed linear neuron network is shown in Table E.3.

	>2500	2000	1600	1250	1000	800	630	500	400	315	250	200	<200
>2500	0.3885												
2000	0.1287	0.0498											
1600	0.1323	0.2014	0.2352										
1250	0.1066	0.2138	0.2584	0.3134									
1000	0.0635	0.1323	0.1667	0.2453	0.3338								
800	0.0459	0.0884	0.0974	0.1557	0.2598	0.3968							
630	0.0355	0.0667	0.0609	0.0873	0.1531	0.2678	0.4759						
500	0.0261	0.0582	0.0463	0.0497	0.0752	0.1346	0.2451	0.5574					
400	0.0196	0.0439	0.0299	0.0293	0.0376	0.0569	0.0982	0.1995	0.6339				
315	0.0136	0.0290	0.0227	0.0281	0.0354	0.0395	0.0528	0.0838	0.1489	0.7508			
250	0.0091	0.0214	0.0183	0.0219	0.0255	0.0256	0.0297	0.0383	0.0606	0.0630	0.8713		
200	0.0093	0.0352	0.0119	0.0039	0.0015	0.0006	0.0062	0.0031	0.0001	0.0542	0.0576	0.9235	
<200	0.0213	0.0600	0.0522	0.0655	0.0780	0.0783	0.0922	0.1179	0.1565	0.1319	0.0711	0.0765	1

Table E.3: Assessed Transition Matrix

The estimated transition Matrix and within it the computed particle size distribution were generally in good agreement with the given ones from Table E.2. The root mean square

error between the given and estimated particle size distribution was 0.00142, which showed that the model was rather well-fitted to obtain a transition matrix.

E.1 Are B and S Matrices unique?

Pettersen and Sandvik/1992[92] have raised the question whether several sets of *S*- and *B*-matrices exist to form the required *A*-matrix? Assuming that *S'* and *B'* are equivalent in terms of a diagonal matrix and a lower triangular matrix respectively – so that they combine into the same *A*-matrix, but different to absolute values of the elements of the "correct" *S* and *B* one can write:

$$(B' - I)S' = (B - I)S \tag{E.1}$$

one then has:

$$(B' - I) = (B - I)S \cdot S'^{-1} \tag{E.2}$$

$$B' = I + (B - I)S \cdot S'^{-1} \tag{E.3}$$

$$B' = BS \cdot S'^{-1} + \left(I - S \cdot S'^{-1}\right) \tag{E.4}$$

B has all diagonal elements equal to zero (besides for $i=j$ = max: b_{ij} = 1), hence the first term is a matrix with all terms equal to zero (besides for $i=j$ = max: equals to 1). Hence all diagonal terms are given by:

$$\left(I - S \cdot S'^{-1}\right) \tag{E.5}$$

Now $S \cdot S^{-1}$ is simply a diagonal matrix with all terms equal to $s_i \cdot s'^{-1}_i$ where s_i and s'_i are the i'th elements of the matrix *S* and *S'*. For *B'*, to have all diagonal terms equal to zero (besides for $i=j$ = max: equals to 1), one clearly requires $s_i \cdot s'^{-1}_i = 1$ (besides for i= max: s_i = 0). This means that the matrix *S'* has to be equal to *S*, and hence that *B'* has to be equal

to *B*. This is contrary to the initial assumption. Hence one may conclude: There is only one *B* and one *S* which together combine in a specific *A* matrix.

To further illustrate the meaning of this we conducted a series of computation for which the selection function was known and compared them with our determined selection. The initial particle size distribution was represented by a vector n_0 the elements of which are equal to 0, except the first one which is equal to 1. The resultant particle size distributions are shown in Table E.4. Upon assuming a randomly generated Selection and Breakage Function matrix we obtained the resultant particle size distribution.

	n_0	n_1	n_2	n_3
1	1	0.977	0.955	0.933
2	0	0.005	0.010	0.014
3	0	0.005	0.010	0.015
4	0	0.004	0.008	0.012
5	0	0.003	0.006	0.009
6	0	0.002	0.004	0.006
7	0	0.002	0.004	0.006
8	0	0.003	0.006	0.009

Table E.4: Particle size distribution

The estimated particle size distributions were computed using the proposed Transition matrix method. The root mean square error between the given and estimated particle size distribution was $5.7 \cdot 10^{-4}$. Using equation (D.2) and equation (D.4) resulted enabled us to compare the given and estimated Selection Function values, which is shown in Table E.5.

S_i	1	2	3	4	5	6	7	8
Assumed	0.023	0.018	0.014	0.010	0.007	0.005	0.003	0
Estimated	0.024	0.019	0.014	0.010	0.007	0.005	0.003	0

Table E.5: Comparison of assumed and estimated Selection Function values

The root mean square error between the given and estimated S_i was 0.0005, which showed that the model is well-fitted to obtain a selection function.

Appendix F: Validation of Approach by Tracer Experiment

A "tracer experiment" was carried out to validate the Markov chain (transition matrix) approach used in this thesis. This experiment was carried out by placing a small amount of "dyed" fibres all of the same length and defect free – as a result of being lab-cooked, into the pulp and subjected this to a small amount of refining.

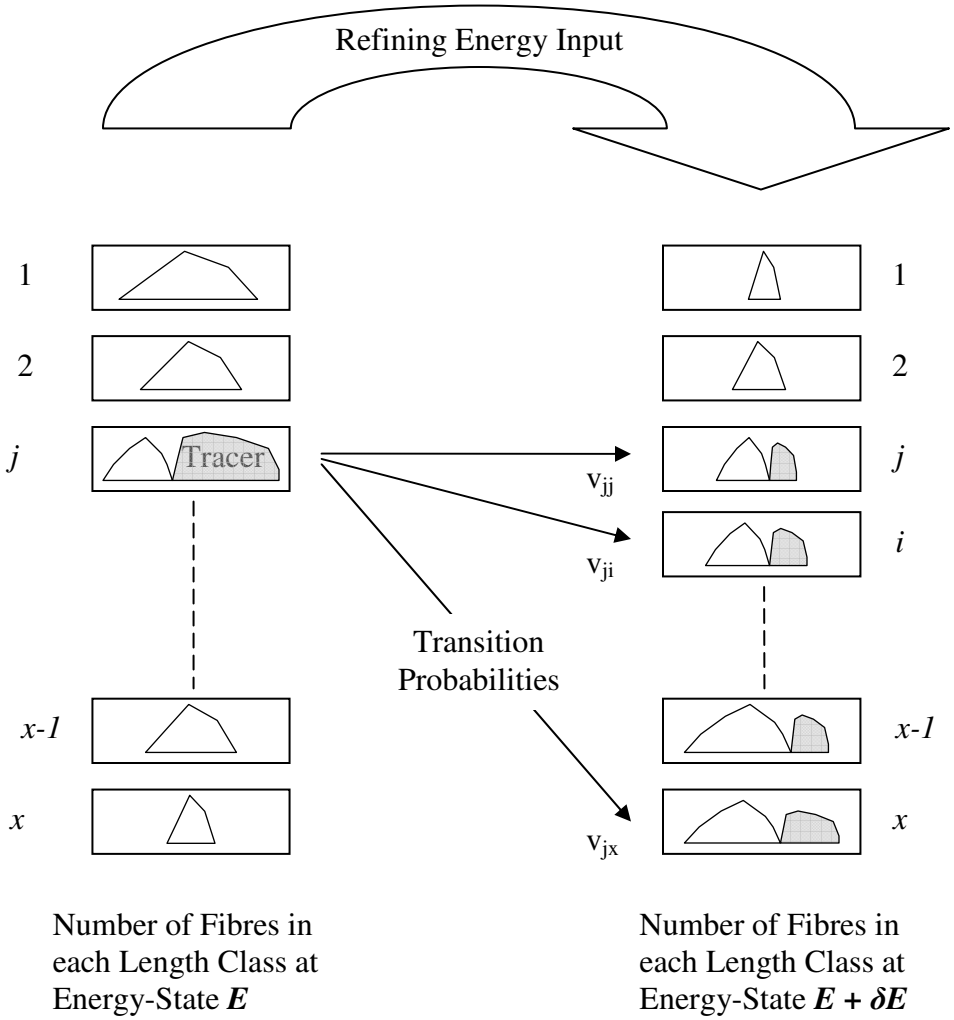

Figure F.1: Stochastic Approach to Batch Refining

For a "tracer experiment" as show in Figure F.1 one can follow all the tracer fibres that belong to class *j* at energy input *E*. Let us note by $n^*_{Tracer,j}(E)$ the fibre length fraction of

the tracer in class j, $n^*_{Tracer,i}(E+\delta E)$ being the fibre length fraction of the tracer in class i after one refining step of energy input δE. For any size fraction j, the probability transition $t(j, i)$ from state j to state i is

$$t(j,i) = \frac{n^*_{Tracer,i}(E+\delta E)}{n^*_{Tracer,j}(E)} \tag{F.1}$$

Based on Bertriaux/2000[84] it can be shown that for this very small energy input, the breakage and selection functions can be estimated:

$$B_{ij} = \frac{n^*_{Tarcer,i}(E+\delta E)}{n^*_{Tarcer,j}(E) - n^*_{Tarcer,j}(E+\delta E)} \tag{F.2}$$

$$S_j = \frac{n^*_{Tarcer,j}(E) - n^*_{Tarcer,j}(E+\delta E)}{n^*_{Tarcer,j}(E)\cdot[E+\delta E - E]} = \frac{1}{\delta E}\cdot\left[1 - \frac{n^*_{Tarcer,j}(E+\delta E)}{n^*_{Tarcer,j}(E)}\right] \tag{F.3}$$

Figure F.1 shows a batch refining process for which the change in fibre length size between energy input t and energy input $E + \delta E$ is determined. Let us assume that refining occurs by elementary steps representing breakage events, an assumption which is made in determining the breakage matrix. For repetitive refining this hypothesis seems to be realistic as a given refiner revolution can be seen as an elementary event. For continuous refining processes, in which breakage occurs through a high intensity of randomly distributed events (in which fibres do not all get treated at the same time), this assumption will still stand as long as interval δE is chosen: not too small to ensure that at least one refining event occurs during this energy interval, and not too big to avoid lack of precision due to the multiplicity of the refining events during δE. As pointed out by Fan et al./1985[93], reducing the elementary energy input factor leads to an increase in the precision of the calculations as it allows a closer approach to a continuous grinding phenomena. However, it can also dramatically increase the calculation time.

Appendix G: Form of Capture Function $f(l_i)$

Below are the various forms of $f(l_i)$ that were explored as best representing the dependence of S_i on fibre length. This was accomplished by least square fitting to minimize differences between the function and length data.

$$f(l_i) = 1 - e^{-k_1 \cdot \frac{l_i}{l_i + D}} \tag{G.1}$$

$$f(l_i) = \frac{l_i}{l_i + k_1 \cdot D} \tag{G.2}$$

$$f(l_i) = 1 - e^{-k_1 \cdot C_F} \cdot e^{-k_2 \cdot \frac{l_i}{l_i + D}} \tag{G.3}$$

$$f(l_i) = \frac{l_i}{l_i + k_1 \cdot D} \cdot \left(1 - e^{-k_2 \cdot C_F}\right) \tag{G.4}$$

$$f(l_i) = 1 - e^{k_1 \cdot C_F} \cdot e^{k_2 \cdot \frac{l_i}{D}} \tag{G.5}$$

$$f(l_i) = \left(1 - e^{-k_1 l_i} \cdot e^{-k_2 C_F}\right) \tag{G.6}$$

$$f(l_i) = \left(1 - e^{-k_1 \cdot \frac{l_i}{D}}\right) \cdot \left(1 - e^{-k_2 \cdot C_F}\right) \tag{G.7}$$

We tested the different equations (G.1) to (G.7) to find the best fit to our length vs. selection function value data. The method of least squares is used to minimize the distance between the input curve points and the theoretical function. As a criteria to choose the appropriate length depended capture function the absolute error between input and theoretical value was used. This was evaluated for all 15 trials. An example for this is shown in Figure G.2: where Trial M and the corresponding graphs representing equations (G.2) and (G.5) are compared. Considering the given lack of knowledge of the refining process and it influential parameter and the result of the above analysis we deem the capture function to be best represented by equation (G.2).

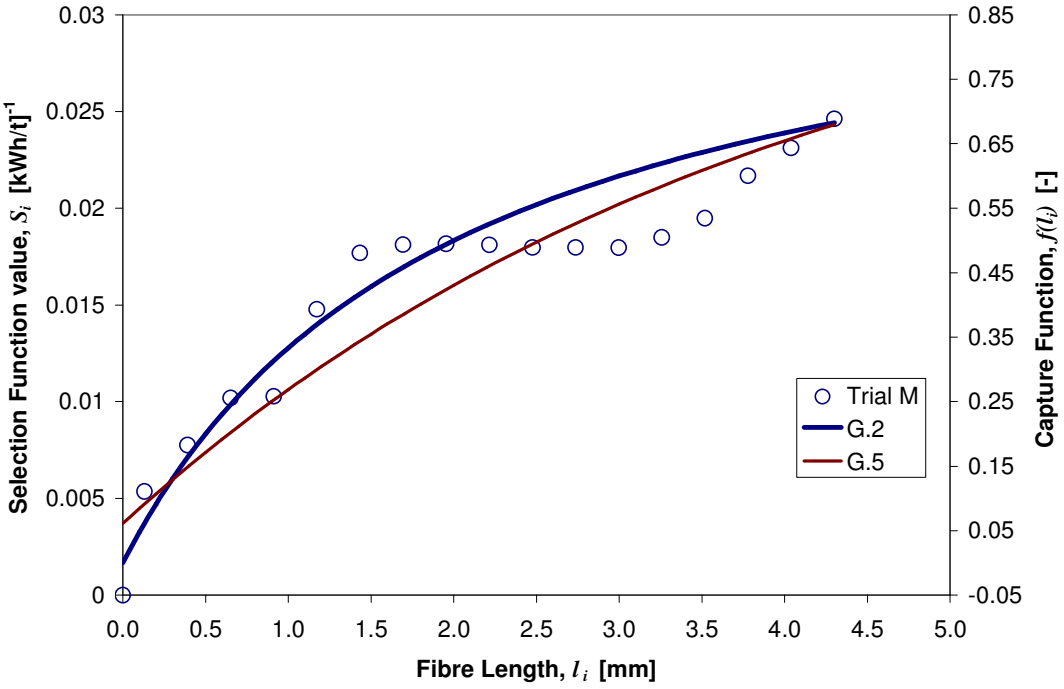

Figure G.2: Comparison of best fit for Capture Function G.2 and G.5 for Trial M